PLOS ONE

RESEARCH ARTICLE

Role of tumor-associated neutrophils in regulation of tumor growth in lung cancer development: A mathematical model

Yangjin Kim[1,2]*, **Donggu Lee**[1], **Junho Lee**[1], **Seongwon Lee**[3], **Sean Lawler**[4]

1 Department of Mathematics, Konkuk University, Seoul, Republic of Korea, **2** Mathematical Biosciences Institute, Ohio State University, Columbus, Ohio, United States of America, **3** Division of Mathematical Models, National Institute for Mathematical Sciences, Daejeon, Republic of Korea, **4** Department of neurosurgery, Harvard Medical School & Brigham and Women's Hospital, Boston, Massachusetts, United States of America

* ahyouhappy@konkuk.ac.kr

Citation: Kim Y, Lee D, Lee J, Lee S, Lawler S (2019) Role of tumor-associated neutrophils in regulation of tumor growth in lung cancer development: A mathematical model. PLoS ONE 14 (1): e0211041. https://doi.org/10.1371/journal.pone.0211041

Editor: Eugene Demidenko, Dartmouth College Geisel School of Medicine, UNITED STATES

Received: August 8, 2018

Accepted: January 7, 2019

Published: January 28, 2019

Data Availability Statement: All relevant data are within the manuscript and its Supporting Information files.

Funding: This work was supported by Konkuk University 2015 Research fund (www.konkuk.ac.kr, Y.J.). The funders had no role in study design, data collection and analysis, decision to publish, or preparation of the manuscript.

Competing interests: The authors have declared that no competing interests exist.

Abstract

Neutrophils display rapid and potent innate immune responses in various diseases. Tumor-associated neutrophils (TANs) however either induce or overcome immunosuppressive functions of the tumor microenvironment through complex tumor-stroma crosstalk. We developed a mathematical model to address the question of how phenotypic alterations between tumor suppressive N1 TANS, and tumor promoting N2 TANs affect nonlinear tumor growth in a complex tumor microenvironment. The model provides a visual display of the complex behavior of populations of TANs and tumors in response to various TGF-β and IFN-β stimuli. In addition, the effect of anti-tumor drug administration is incorporated in the model in an effort to achieve optimal anti-tumor efficacy. The simulation results from the mathematical model were in good agreement with experimental data. We found that the N2-to-N1 ratio (N21R) index is positively correlated with aggressive tumor growth, suggesting that this may be a good prognostic factor. We also found that the antitumor efficacy increases when the relative ratio (Dap) of delayed apoptotic cell death of N1 and N2 TANs is either very small or relatively large, providing a basis for therapeutically targeting prometastatic N2 TANs.

Introduction

Lung cancer is the leading cause of cancer mortality worldwide, with an approximate 1.6 million deaths each year [1]. The most common ($\sim$85%) form of lung cancer in patients is non-small cell lung cancer (NSCLC), of which lung squamous cell carcinoma (LUSC) and lung adenocarcinoma (LUAD) are the most common subtypes [2]. Various groups of myeloid cells have been known to promote tumor development by direct inhibition of immune responses [3], as well as by secreting growth factors, angiogenic factors, or matrix-degrading enzymes [4, 5]. For example, tumor-associated macrophages (TAMs), also known as M2 macrophages [3], have been shown to promote tumor growth [6, 7]. There is growing evidence suggesting that

neutrophils play a major role in tumor progression from establishment of tumor formation and throughout the progression to the malignant state [8–12]. For example, tumor associated neutrophils (TANs) have been associated with poor prognosis in many cancers including metastatic melanoma [13], bronchoalveolar carcinoma [14], and renal carcinoma [15]. Like TAMs, TANs infiltrate tumor tissue and can have two differential states in cancer progression [8, 9, 16]: (i) an antitumorigenic role (called N1) (ii) promoting tumor progression (called N2). How these two phenotypes are regulated is largely unknown but many experimental and clinical findings suggest the significant potential of therapeutic targeting of the prometastatic role of TANs [17].

TGF-β has been identified as a major cytokine within a tumor that skews neutrophil differentiation toward the N2 phenotype [16, 18, 19], while TGF-β blockade and type-1 IFN (α, β, ω) treatment are known to shift the balance toward the N1 phenotype [20, 21]. IFN-β in tumor microenvironment can directly suppress tumor growth [22] by interacting with p53 [23–25]. IFN treated neutrophils were shown to upregulate PD-L1 and suppress T-cell proliferation [26]. After binding to interferon receptor type 1, IFNAR1 and IFNAR2, Type 1 IFN-β signals through TYK2 and JAK1, which in turn phosphorylate STAT family members (STAT1, STAT2, STAT3, and others) and activate its downstream functions to stimulate anti-tumor activities [27]. For example, vesicular stomatitis virus expressing IFN-β was shown to enhance anti-tumor immune responses in a murine model of NSCLC [28]. It is well established that cancer associated fibroblasts (CAFs) can promote tumor growth, aggressive invasion, and metastasis through mutual interaction in the tumor microenvironment [29, 30]. Fibroblast-secreted IFN-β was also able to restrict expression of the p53 RNA stabilizer, WIG1, and bring down mutant p53 RNA levels, thus suggesting an alternative therapeutic agent for mutant p53 positive lung cancer patients [31]. There are multiple levels of crosstalk between neutrophils and many cells including other immune cells and Th17 cells [32]. Neutrophils may express many important factors such as IL-6, IL-17A, IL-17F and IFNγ [33]. How neutrophils are induced by a tumor is still poorly understood. It is well known that tumor cells interact with stromal cells such as fibroblasts, immune cells (neutrophils, macrophages, Th17, Tregs, T cells), and cytokines in the tumor microenvironment, and that these complex interactions play a critical role in tumor initiation, growth, angiogenesis, and metastasis. The mutual interactions between a tumor and immune system involving TANs are summarized in Fig 1 with references in Table 1.

In this work, we employed the framework of the differential equation model in order to take into account the role of N1 and N2 TANs in the regulation of tumor-neutrophil interactions and tumor growth. Based on a schematic diagram in Fig 2, the model consists of a system of ordinary and delay differential equations involving the following variables:

$$\begin{aligned} C(t) &= \text{ density of the N2 complex at time } t, \\ I(t) &= \text{ density of the N1 complex at time } t, \\ T(t) &= \text{ density of tumor cells at time } t. \end{aligned}$$

TGF-β and IFN-β play a central role in the critical transition between N1 and N2 TANs, resulting in either tumor-promoting or tumor-suppressing microenvironment. We summarize in Fig 3 the fundamental, phenotypic spectrum underlying how the oncogenic and tumor suppressive properties of TANs arise in relation to TGF-β, IFN-β, and delayed apoptotic cell death mechanisms. This model is then used (i) to investigate how TGF-β and IFN-β regulate the balance between N1 and N2 phenotypes by complex mutual interactions, (ii) to investigate how up- or down-regulation of these N1 and N2 phenotypes affect tumor growth and anti-tumor

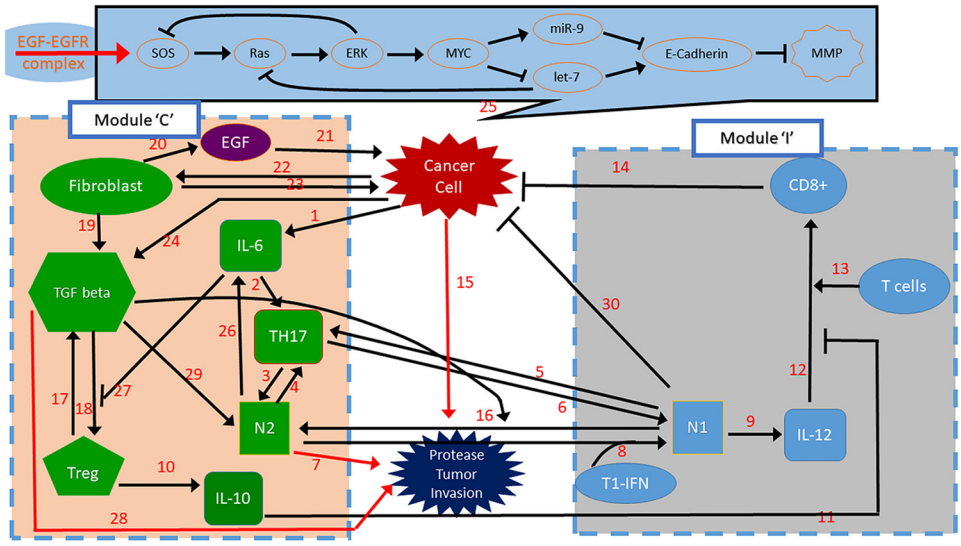

Fig 1. A schematic of tumor-microenvironment interaction. (Top) A signaling pathway for lung cancer. (Bottom) Network of interactions between cells involved (cancer cells, fibroblasts, Th17 cells, N1 cells, N2 cells, CD8+ T cells, Tregs) and cytokines and growth factors (EGF, IL-6, IL-10, IL-12, MMPs, TGFβ). By convention, the kinetic interpretation of solid arrows and hammerheads in the interaction network represents induction (arrow) and inhibition (hammerhead), respectively. The module on the left and right will be represented by a module 'C' and 'I', respectively, in our simplified mathematical model. References for each interaction (number on the arrow or hammerhead) are provided in Table 1.

https://doi.org/10.1371/journal.pone.0211041.g001

efficacy in the absence and presence of delayed apoptotic cell death mechanisms, and (iii) to develop optimal strategies of the combination therapy with TGF-β inhibitor and IFN-β.

Materials and methods

Mathematical model

N1 module and N2 complex. In this work, we assume: (i) High levels of TGF-β and IL-6 induce upregulation of the N2 complex [8, 34]. (ii) High IFN-β levels induce upregulation of the N1 phenotype [8]. (iii) Cells in the N1 and N2 complex have natural decay at rates μ_{N1}, μ_{N2}, respectively. (iv) Those factors in (i) and (ii) determines the critical transition between N1 and N2 complexes [35], determining either promotion or suppression of tumor growth.

In order to incorporate the signaling network into a mathematical model we simplified the network shown in Fig 4A as follows: We merged the N2 regulatory network among Treg, Th17 and N2 cells into one component (N2 complex; brown dashed box in Fig 4A) while we merged the immune regulatory network of N1 cells, IL-12 and CD8+ (N1 complex; blue dashed box in Fig 4A) in a separate module. The mathematical model network is shown in Fig 4B. By convention, the kinetic interpretation of solid arrows and hammerheads in the signaling network represents induction (arrow) and inhibition (hammerhead), respectively.

Let the variables $N_2(t)$ and $N_1(t)$ be activities of the N2 complex and N1 module, respectively, at time t. The scheme includes autocatalytic activities of the N2 complex (N_2) and N1 complex (N_1), removal of those key cells in the tumor microenvironment, mutual inhibition between those two modules, and clearance/decay of those complexes.

The mass balance (or conservation of mass) of a physical variable states that the rate of change of this quantity is the sum of contributing factors such as an input factor with the positive sign and an output factor with the negative sign. Therefore, the mass balance of the

Table 1. Summary of interaction networks (Fig 1) in invasion processes in lung cancer development.

#	Description	References
1	cancer cells secrete IL-6	[157]
2	In combination with TGF-beta, IL-6 promotes the differentiation of Th17 cells by activating transcription factors including retinoic acid-related orphan receptor RORγt and RORα	[158–160]
3	IL17 can indirectly induce the recruitment of neutrophils.	[32, 102]
4	Neutrophils secrete chemokines that can mediate the recruitment of Th17 cells and. secrete IL-17	[33, 102]
5, 6	IL17 can indirectly induce the recruitment of neutrophils	[32]
7	Neutrophils release TIMP-free MMP-9, MMP infiltration supplies MMP-9, Intravenous co-injection of mammary adenocarcinoma cells and neutrophils significantly raises lung metastases, N2 phenotype induces angiogenesis, invasion and metastasis, and maintain immunosuppression [161]	[161, 161–166]
8	Type I IFNs (or IFN*beta*) induce anti-tumor polarization, N2 TAN, in mice and human	[20, 21]
9	Neutrophils secrete/induce IL-12	[97, 99, 167]
10, 11	Tregs can inhibit tumor-specific CD8+ (54) and CD4+ (55) T cell effector functions through IL-10	[168–173]
12, 13	N1 Neutrophils promote recruitment and activation of CD8(+) cells by producing cytokines (IL-12, TNFα, GM-CSF, VEGF)	[97]
15, 23	Cancer associated fibroblasts (CAFs) promote tumor growth, aggressive invasion, and metastasis	[29, 30]
16	TGF-β within the tumor microenvironment induces TAN with a pro tumor phenotype. TGF-β blockade results in the recruitment and activation of TANs with an anti tumor phenotype	[16, 18, 19]
17	Tregs can inhibit tumor-specific CD8+ (54) and CD4+ (55) T cell effector functions through TGFβ	[168–174]
18	TGF-β induces Foxp3+ T-reg from CD4+CD25	[160, 161, 175–177]
19	CAF secretes TGF-β and VEGF for Treg induction	[177, 178]
20, 21	CAF secretes EGF, which in turn promotes tumor growth and invasion	[41, 47, 64, 152, 178, 179]
22, 23	Lung cancer cells recruit CAFs and CAFs induce tumor growth, chemoresistance, angiogenesis, metastasis	[178]
24	Cancer cells change tumor microenvironment by secreting TGF-β	[178]
25	RAS-let-7-miR-9 signaling network induce lung cell invasion	[180–187]
26	N2 TANs expressed TGFbeta and IL-6	[8, 103, 104, 188]
27	IL-6 inhibits the generation of Treg cells and induces production of IL-17	[160]
28	IL-6 enhanced epithelial cell EMT and stimulated tumor progression by enhancing TGFβ signaling. IL-6 and TGFβ plays a central role in regulation of the paracrine loop between these two cytokines in LSCLS, TGFβ exposure induces EMT in CSCs and non-CSCs	[189, 190]
29	"Neutrophils are driven by transforming growth factor-β (TGFβ) to acquire a polarized, pro-tumoural N2 phenotype (characterized by high levels of arginase expression)."	[33]
30	Neutrophils have cytotoxic mediators for tumor cell killing such as TNF-α, IL-1β, and IFNs	[161, 191]

https://doi.org/10.1371/journal.pone.0211041.t001

densities of the N2 module (N_2) and N1 module (N_1) leads to a system of ordinary differential equations (ODEs) as follows:

$$\frac{dN_2}{d\tau} = f_1(\lambda_{IL-6}, g) + \frac{a_1 a_3^2}{a_3^2 + a_4 F(N_1)} - \mu_{N2} N_2, \tag{1}$$

$$\frac{dN_1}{d\tau} = f_2(s) + \frac{a_2 a_5^2}{a_5^2 + a_6 H(N_2)} - \mu_{N1} N_1. \tag{2}$$

The first term in Eq (1) represents the signaling from N2-promoting molecules such as IL-6 and TGF-β. Similarly, the first term in Eq (2) represents the signaling from N1-promoting molecules such as IFN-β. The third terms in Eqs (1) and (2) indicate natural decay/consumption of N2 and N1 complexes, respectively. The second term in Eq (1) represents autocatalytic

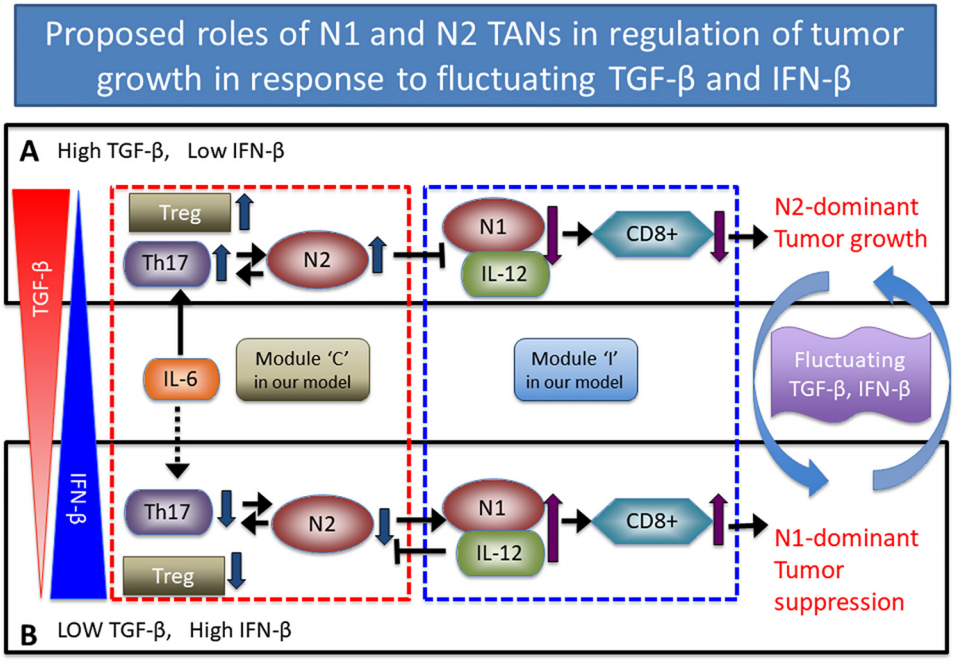

Fig 2. Proposed role of N1 and N2 complexes in the regulation of tumor growth and immune-suppression in response to fluctuating TGF-*β* and IFN-*β*. The phenotypic balance between N1 and N2 complexes determines tumor growth or suppression in response to TGF-*β* (red triangle on the left) and IFN-*β* (blue triangle on the left). (A) High TGF-*β* levels and low IFN-*β* activities induce Treg infiltration which in turn leads to biochemical suppression of the overall anti-tumor immune activities of T cells. TGF-*β* also modifies the tumor microenvironment by transforming N1 into N2 TANs [8, 34] while IFN-*β* brings the N2 phenotype back to the N1 phenotype [8]. This N2-dominant microenvironment leads to enhanced tumor growth. (B) Low TGF-*β* levels and upregulation of IFN-*β* reduce the phenotypical transition from N1 to N2 TANs and leads to upregulation of immune activities of T cells and N1 TANs, leading to suppression of tumor growth. Schematic components of the N2/Th17/Treg complex and the N1/IL12/CD8+ complex are represented by modules 'C' (box with the red dotted line) and 'I' (box with the blue dotted line) in our theoretical framework. Blue arrows on the right indicate the switching behavior between a tumor-promoting mode in (A) and the tumor-suppressive state in (B) in response to fluctuating TGF-*β* and IFN-*β* levels.

https://doi.org/10.1371/journal.pone.0211041.g002

enhancement of the N2 module (numerator) with inhibition from the N1 module (denominator). The second term in Eq (2) is defined in a similar fashion. In more detail, $f_1(\lambda_{IL-6}, g)$ is a positive function that represents the signaling pathways from cancer-induced IL-6 (λ_{IL-6}) and cancer-induced TGF-*β* (g) to the N2 module, $f_2(s)$ is a function that represents the signaling pathways from IFN-*β* (s) to the N1 complex, a_1, a_2 are the autocatalytic enhancement parameters for the N2 and N1 modules, respectively, a_3, a_5 are the Hill-type inhibition saturation parameters from the counter part of N2 and N1 complex, respectively, a_4 is the inhibition strength of the N2 complex by the N1 TANs, a_6 is the inhibition strength of the N1 module by the N2 module, and finally μ_{N2}, μ_{N1} are the clearance/death rate of N2 and N1 complexes, respectively.

As indicated in Eq (1), the signals λ_{IL-6} and g increase the rate of N2 activation through the function $f(\lambda_{IL-6}, g)$ in the first term, while N1-dependent inhibition of the N2 complex is expressed through the function $F(N_1)$ in the denominator of the second term. A simple requirement of these functions is that the function has to be an increasing function of the factor molecules. For example, the signaling function of the N2 complex ($f_1(\lambda_{IL-6}, g)$) increases as the signaling of IL-6 (λ_{IL-6}) and TGF-*β* (g) increases, and the inhibition strength of the N2 complex by the N1 complex, $F(N_1)$, increases as the N1 population (N_1) increases. In other words, $\frac{\partial f_1}{\partial \lambda_{IL-6}} > 0$, $\frac{\partial f_1}{\partial g} > 0$ for all non-negative λ_{IL-6} and g, and $\frac{\partial F}{\partial N_1} > 0$ for all non-negative N_1.

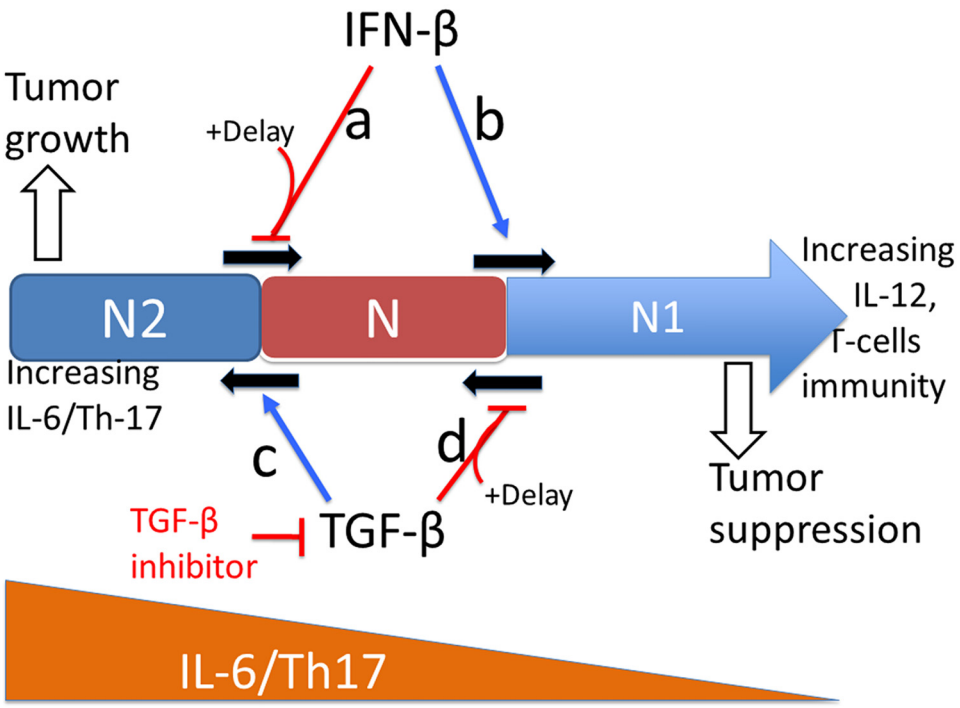

Fig 3. Tumor suppressive and tumor promoting roles of TGF-β and IFN-β respectively in the tumor microenvironment. As the CD8+ cytokines (IL-12) increase, differentiation of N cells transits to the N1 phenotype. There are three ways that IFN-β, TGF-β inhibitor, and delayed apoptotic pathways can keep the system in the safe-guard immune N1 zone. (Cases a, b) Increasing IFN-β levels induces the transition from N2 to N1-zone (case b) [22–25, 35–37]. The delayed apoptotic cell death of N2 TANs suppresses entry into the transition phase (case a). (Cases c, d) As the IL-6 level is increased (to the left), the tumor-promoting phenotype, N2, becomes dominant and TGF-β promotes the exit from the transition zone to enter the N2-zone (case c) [35]. The TGF-β inhibitor can reverse the phenotype back to the N1 microenvironment [38]. The delayed apoptotic cell death of N1 TANs suppresses entry into the transition phase (case d).

https://doi.org/10.1371/journal.pone.0211041.g003

Similarly, the first term $f_2(s)$ on the right-hand side of Eq (2) represents an increase in N1 activity induced by the signal s, and N2-dependent suppression of N1 activity is explored through the function $H(N_2)$ in the denominator. The signaling function of the N1 complex ($f_2(s)$) increases as the signaling of IFN-β (s) increases, and the inhibition strength of N1 complex by N2 complex, $H(N_2)$, increases as the N2 population (N_2) increases. In other words, $\frac{\partial f_2}{\partial s} > 0$, $\frac{\partial H}{\partial N_2} > 0$ for all non-negative s, N_2. Based on biological observations (Fig 4A), we assume that

$$\begin{aligned} f_1(\lambda_{IL-6}, g) &= \lambda_{IL-6} + \lambda_{TGF-\beta} g, \quad & F(N_1) &= N_1^2, \\ f_2(s) &= \lambda_{IFN\beta} s, & H(N_2) &= N_2^2, \end{aligned} \tag{3}$$

where $\lambda_{TGF-\beta}$ is the TGF-β-induced signal rate and $\lambda_{IFN\beta}$ is the IFN-β -induced signal rate.

After performing the following non-dimensionalization

$$\begin{aligned} & t = \mu_{N2}\tau,\ C = \frac{N_2}{N_2^*},\ I = \frac{N_1}{N_1^*},\ \lambda = \frac{\lambda_{IL-6}}{\mu_{N2} N_2^*},\ G = \frac{g}{G^*},\ \lambda_G = \frac{\lambda_{TGF-\beta} G^*}{\mu_{N2} N_2^*}, \\ & \mu = \frac{\mu_{N1}}{\mu_{N2}},\ S = \frac{s}{S^*},\ \lambda_S = \frac{\lambda_{IFN\beta} S^*}{\mu_{N2} N_1^*},\ k_1 = \frac{a_1 a_3^2}{\mu_{N2} N_2^*},\ k_3 = a_3,\ k_2 = \frac{a_2 a_5^2}{\mu_{N2} N_1^*}, \\ & k_4 = a_5,\ \alpha = a_4 (N_1^*)^2,\ \beta = a_6 (N_2^*)^2, \end{aligned} \tag{4}$$

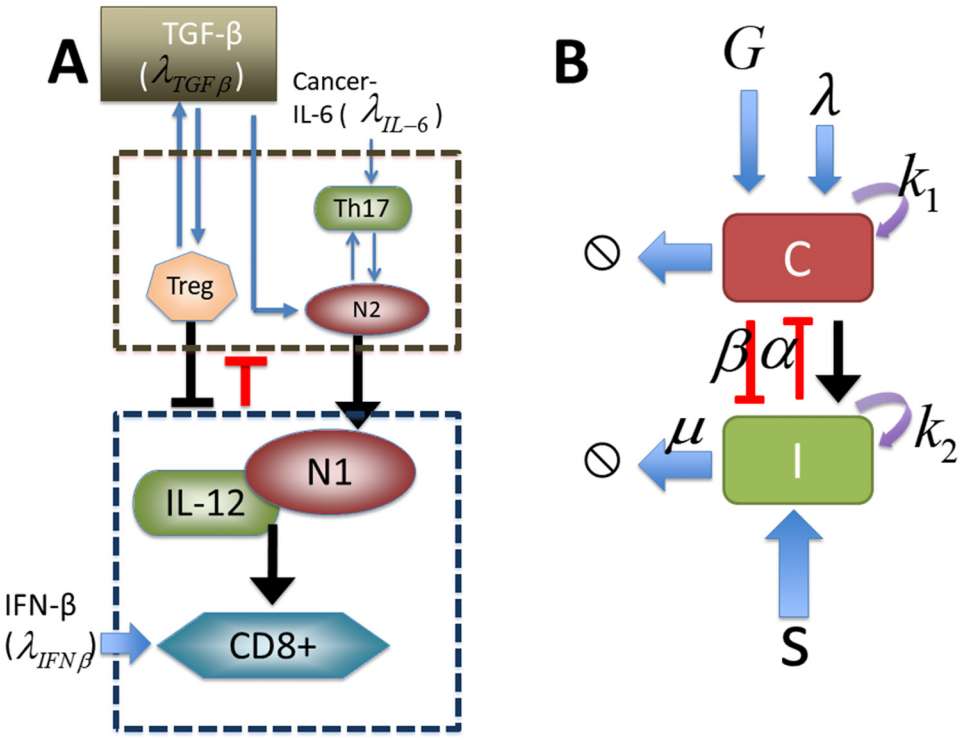

Fig 4. A schematic of our mathematical model.

https://doi.org/10.1371/journal.pone.0211041.g004

from the dimensional Eqs (1)–(3), we obtain the associated dimensionless equations for N2 (C) and N1 (I) complexes with a set of essential control parameters:

$$\frac{dC}{dt} = \lambda + \lambda_G G + \frac{k_1}{k_3^2 + \alpha I^2} - C, \tag{5}$$

$$\frac{dI}{dt} = \lambda_S S + \frac{k_2}{k_4^2 + \beta C^2} - \mu I. \tag{6}$$

Tumor volume ($T(t)$). As we discussed above, neutrophils play either tumorigenic or anti-tumorigenic roles in response to various biochemical signals such as TGF-β and IFN-β in a complex microenvironment. While N1 TANs kill tumor cells [8], N2 TANs promote tumor growth [8, 35]. Therefore, tumor growth and tumor cell killing are promoted or suppressed by relative balance between N1 and N2 TANs [8], which, in our model, is determined by dichotomous polarization of neutrophils (either N2 TANs (C) or N1 TANs (I)) in Eqs (3)–(6) in response to microenvironmental signals such as IL-6 (λ), TGF-β (G) and IFN-β (S). Gompetz growth, logistic growth, and other nonlinear growth curves have been suggested to fit to the experimental data on tumor growth [39]. Logistic growth in the absence and presence of growth factor-mediated enhancement of tumor growth has been observed in experiments [40–44] and mathematical models were successfully applied to predict these experimental results [7, 40–51]. We assume that (i) the tumor grows at a basic rate r in the absence of promotion of N2 TANs (C) and tumor cell killing by N1 TANs (I), following logistic growth, (ii) tumor growth is enhanced in a N2-mediated tumor microenvironment, (iii) anti-tumorigenic

N1 TANs kill the tumor cell at a rate δ. In particular, the N2-mediated enhancement of tumor growth is modeled by a fraction of the N2 phenotype (C) relative to the N1 phenotype (I) in tumor microenvironment:

$$\frac{C}{K+\gamma_1 I}$$

where K, γ_1 are the inhibition parameters of N2-mediated growth.

The mass balance of the tumor volume (T) leads to an ordinary differential equation as follows:

$$\frac{dT}{dt} = r\left(1+\frac{C}{K+\gamma_1 I}\right)T\left(1-\frac{T}{T_0}\right) - \delta\ I\ T, \tag{7}$$

where r is a growth rate of the tumor and T_0 is the carrying capacity of the tumor population.

All simulations were performed using Matlab (Mathworks) for ordinary differential equations (ode45) and delay differential equations (dde23).

Parameter estimation

μ_{N1}, μ_{N2}: Neutrophil turnover in blood is quite rapid [52]. The half-life of neutrophils within the circulation ($T_{1/2}$) was reported to be 3.2 hours in rabbits [53, 54], 11.4 hours in mice [55], and 7-10 hours in humans [56, 57]. On the other hand, the measured half-life in *in vivo* experiments [58] was measured to be longer: 90 h in vivo experiments [59], 20.3 in neutropenia patients [60], and 17.3 h in terminal cancer patients with glioblastoma and chronic lymphocytic leukemia [61]. For example, Andzinski *et al.* [62] recently reported that the life span of TANs can be remarkably prolonged in tumor microenvironment where IFN-β activity is suppressed [63]. Based on these biological observations in the tumor microenvironment, neutrophils in tumor tissue, we take the half-life of about $T_{1/2} = 20\ h$. In general, we can obtain the decay rate of a variable when we know the half-life. In more detail, by solving a typical differential equation of the form $\frac{dy}{dt} = -\lambda y$ with an initial condition $y(0) = y_0$ and a delay rate λ, and comparing the solution $y(t) = y_0 e^{-\lambda t}$ at $t = T_{1/2}$, we can obtain the decay rate $\lambda = \frac{\ln(2)}{T_{1/2}}$. This calculation then leads to $\mu_{N2} = \frac{ln(2)}{20h} \sim 0.035h^{-1}$. We also take $\mu_{N1} = \mu_{N2}$.

μ_G: The decay rate of TGF-β was estimated to be $8.02 \times 10^{-6}\ s^{-1} = 2.89 \times 10^{-2}\ h^{-1} = 6.929 \times 10^{-1}\ day^{-1}$ [7, 41, 47, 64]. Thus, dimensionless $\mu_G = 2.89 \times 10^{-2}\ h^{-1}/(0.035h^{-1}) = 0.826$.

μ_L (decay rate of TGF-β inhibitor): The half-life of galunisertib, TGF-β inhibitor, was measured to be 0.53 h in rat, 0.3 h in mice, 2.26h in dogs [65]. We take $\mu_L = 3\ h$, leading to $\mu_L = ln(2)/(3h) = 2.31 \times 10^{-1}\ h^{-1}$. Thus, dimensionless $\mu_L = 2.31 \times 10^{-1}\ h^{-1}/(0.035h^{-1}) = 6.6$.

μ_S (decay rate of IFN-β): The serum half-life of IFN-β ranges from minutes to hours depending on biological conditions of its receptors in response to intravenous injection in mice [66]. The distribution and terminal half-lives were measured to be 5 min and 5 h in healthy male volunteers (N = 12) [67]. We take $\mu_S = 5\ h$, leading to $\mu_S = ln(2)/(5h) = 1.386 \times 10^{-1}\ h^{-1}$. Thus, dimensionless $\mu_S = 1.386 \times 10^{-1}\ h^{-1}/(0.035h^{-1}) = 3.96$.

G^*: The TGF-β level in the lung cancer microenvironment was measured to be in the range of $400 - 2,000\ pg/mL$ [38]. We take $G^* = 1,000\ pg/mL$.

S^*: Deng *et al.* [68] investigated the effect of STING-dependent cytosolic DNA sensing on the IFN-β-dependent anti-tumor efficacy with the control IFN-β concentration of 10 ng/mL and IFNγ value of 20 ng/mL. We take $S^* = 10\ ng/mL$.

Table 2 summarizes all the essential parameter values in the system (5)–(7).

Table 2. Parameters used in the model.

Par	Description	Value	Refs
	N1/N2 modules		
λ	IL-6-induced signaling source of the N2 module	0.01	[103], Estimated
G	TGF-β-induced signaling source of the N2 module	0-1.0	[38]
k_1	autocatalytic production rate (N2 module)	4.0	Estimated
k_3	Hill-type coefficient	1.0	Estimated
α	Inhibition strength of the N2 module by the N1 module	1.5	Estimated
k_2	autocatalytic production rate (N1 module)	4.0	Estimated
k_4	Hill-type coefficient	1.0	Estimated
β	Inhibition strength of the N1 module by the N2 module	1.0	Estimated
S	IFN-β-induced signaling source of the N1 module	0-1.0	[68], Estimated
μ	Relative decay rate of N1 and N2 TANs	1.0	[60, 61]
th_C	Threshold of the N2 module for tumor growth switch	1.5	Estimated
	Tumor module		
r	Tumor growth rate	0.05	[36]
K	Inhibition parameter of N2-mediated growth	1.0	[36], Estimated
γ_1	Inhibition parameter of N2-mediated growth	0.1	[36], Estimated
T_0	Carrying capacity of a tumor	100	[36], Estimated
δ	Killing rate of tumor cells by N1 TANs	0.005	[36], Estimated
	Therapeutics		
G_s	TGF-β source	0.826	Estimated
μ_G	Decay rate of TGF-β	0.826	[7, 41, 47, 64].
γ_L	Clearance rate of TGF-β from TGF-β inhibitor binding	100	Estimated
L_s	Injection rate of TGF-β inhibitor	13	Estimated
μ_L	Decay rate of TGF-β inhibitor	6.6	[65]
S_S	IFN-β injection rate	1 -100	[22–25, 36, 37]
μ_S	Decay rate of IFN-β	3.96	[67]
	Reference values		
G^*	TGF-β Concentration	1 ng/mL	[38]
S^*	IFN-β Concentration	10 ng/mL	[68]
T^*	Tumor Volume	100 mm^3	[36]

https://doi.org/10.1371/journal.pone.0211041.t002

Results

Dynamics of the model

We first investigated the local dynamics of the system (5) and (6). By taking different initial values of N1 and N2 complexes and numerically solving Eqs (5) and (6), one can obtain solutions $(C(t), I(t))$ at time t and plot the relative locations of solutions in the $C - I$ domain. In Fig 5 we illustrate three different flow patterns of the system (5) and (6) near the equilibrium point (steady state (SS); circles) in response to low ($G = 0.1$ in Fig 5A), intermediate ($G = 0.4$ in Fig 5B), and high ($G = 1.0$ in Fig 5C) TGF-β levels in the $C - I$ phase diagram. We note that if the equilibrium point is *stable*, the solution converges to the stable SS (called *attractor*). On the other hand, when the equilibrium point is *unstable*, the solution does not converge to the unstable SS and the solution is repelled by the unstable SS (called *repeller*). By taking the thresholds, C^{th} (= 1.5) for the N2 level and I^{th} (=1.5) for the N1 level, we shall define the anti-

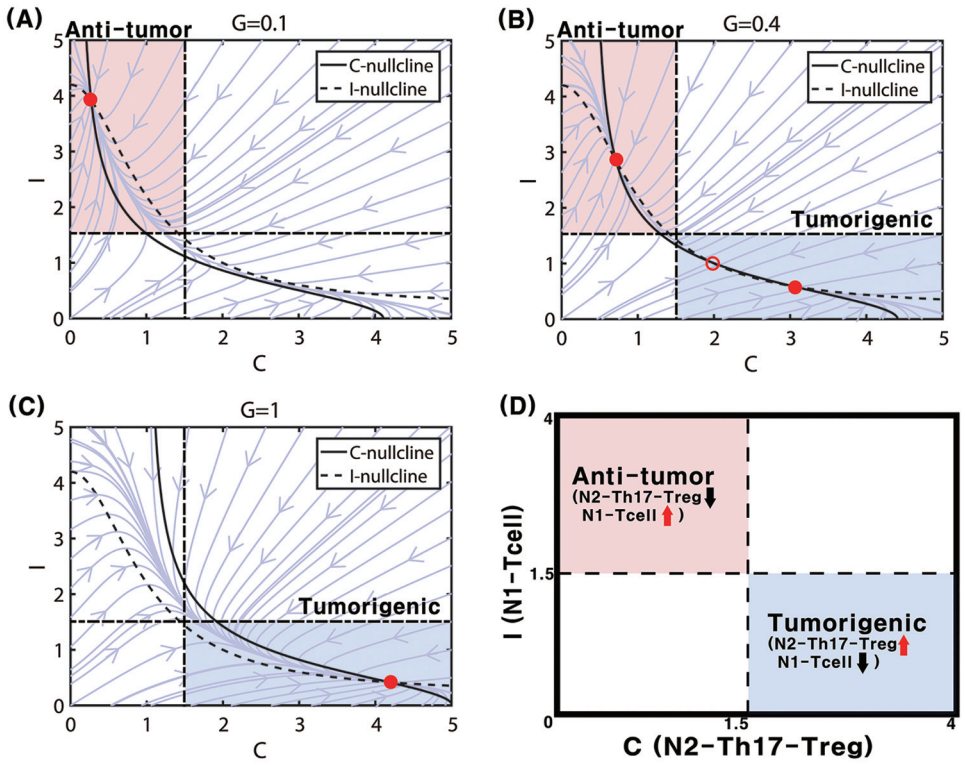

Fig 5. Nonlinear dynamics. Dynamics of the system (5) and (6) in the C-I phase plane in response to low ($G = 0.1$ in (A)), intermediate ($G = 0.4$ in (B)), and high ($G = 1.0$ in (C)) levels of TGF-β-induced transition signals. Steady states marked with circles (stable steady state = filled circle, unstable steady state = empty circle). (D) A schematic of anti-tumorigenic ($C < C^{th}$, $I > I^{th}$) and tumorigenic ($C > C^{th}$, $I < I^{th}$) regions in the $C - I$ plane. $S = 0.2$ fixed. Other parameters are given in Table 2.

https://doi.org/10.1371/journal.pone.0211041.g005

tumorigenic ($\mathbb{P}_a$) and tumorigenic ($\mathbb{P}_t$) phases as follows:

$$\mathbb{P}_a = \{(C, I) \in \mathbb{R}^2 : C < C^{th}; I > I^{th}\}$$
$$\mathbb{P}_t = \{(C, I) \in \mathbb{R}^2 : C > C^{th}; I < I^{th}\}.$$

Fig 5D illustrates the anti-tumorigenic (low activities of the N2 module, high activities of N1 TANs) and tumorigenic (high activities of the N2 complex, low activities of the N1 complex) in a $C - I$ plane. A low TGF-β level ($G = 0.1$) induces only one stable SS (Fig 5A) where suppression of N2 activities and promotion of N1 activities induce the anti-tumorigenic status ($\mathbb{P}_a$). In this case, the environment eventually induces the anti-tumorigenic phenotype regardless of initial status of N1 and N2 complexes. In contrast, the increased activity of N2 TANs, and decreased activity of N1 TANs, leading to the tumorigenic phase ($\mathbb{P}_t$), are induced under a high TGF-β condition ($G = 1.0$; Fig 5C; one stable SS). In this case, the environment eventually induces the tumorigenic phenotype regardless of initial status of N1 and N2 complexes. For an intermediate level of TGF-β signals ($G = 0.4$), there exist three equilibria: two stable SS (two filled circles; one in $\mathbb{P}_t$ and one in $\mathbb{P}_a$) and one unstable SS (empty circle) in the middle. This leads to a bi-stable system shown in Fig 5B. In this case, the environment will induce either anti-tumorigenic or tumorigenic phenotype depending on the initial status of N1 and N2 complexes. From these observations, we anticipate to see a bifurcation curve, especially hysteresis, *i.e.,* the N2 level with TGF-β signal parameter G.

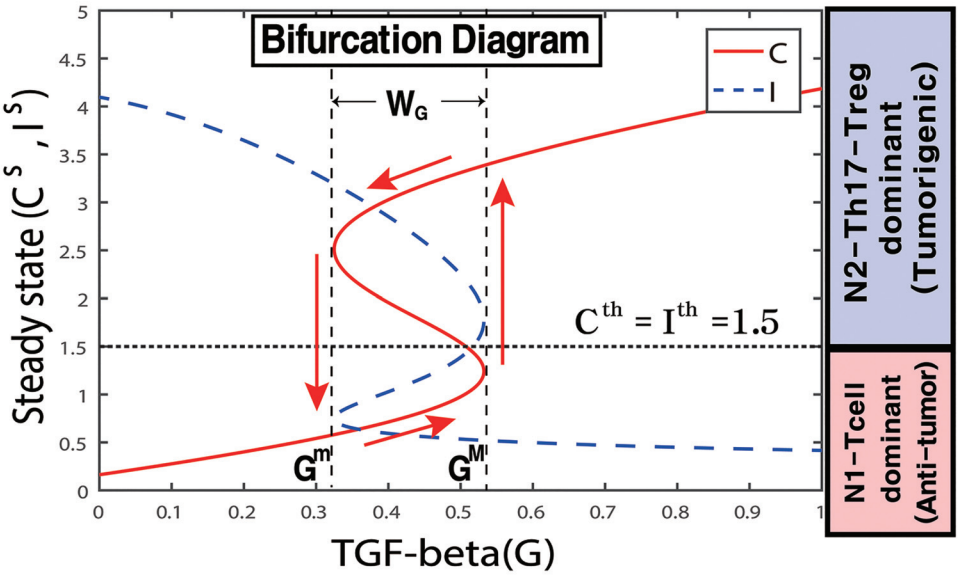

Fig 6. Bifurcation diagram. High and low TGF-β signals (G) provide an on-off switch of N2 activation and determine the dichotomous behavior: cancer cell activation and benign status. Y-axis = steady state (SS) of levels of the N2 (C) and N1 (I) complex modules. $W_G = [G^m, G^M]$ = a window of bi-stabilty. $S = 0.2$. Other parameters are given in Table 2.

https://doi.org/10.1371/journal.pone.0211041.g006

Effect of TGF-β on transitions between N1/N2 TANs and tumor growth

When the system (5) and (6) is in equilibrium, we can solve C as a function of the TGF-β signal (G). Fig 6 shows the graphs $C = C(G)$ and $I = I(G)$ as a hysteresis. While the upper and lower branches are stable, the middle branch is unstable (recall the G-dependent stability in Fig 5). If G is small, then the system is in the lower branch (C low, I high), leading to the anti-tumorigenic phase ($\mathbb{P}_a$). This situation continues to hold as G is increased until it reaches the right knee point of the curve (when $G = 0.53$). At this point, the N2 level jumps to the high branch, with an elevated level of N2 TANs, leading to the tumorigenic phase ($\mathbb{P}_t$). As G is decreased, the N2 level remains elevated, until G is decreased to the left knee point of the curve (when $G = 0.33$), at which time the N2 level jumps down to the lower branch, and the system returns to the cancer-free mode ($\mathbb{P}_a$). We conclude that the effect of G is history dependent: when G is at an intermediate level ($0.33 = G^m < G < G^M = 0.53$; bi-stable mode in Fig 5B), the system induces the anti-tumor phase $\mathbb{P}_a$ if G is in an increasing mode from the low G value, and leads to the tumor-promoting phase $\mathbb{P}_t$ if G is in decreasing mode from the high G level. The bifurcation diagram in Fig 6 suggests that a state (G, C) with $C > C^{th} = 1.5$ will be moved by the dynamical system (5) and (6) into the upper stable steady state branch, resulting in prevailing $\mathbb{P}_t$-status. On the other hand, if $C < C^{th} = 1.5$, then (G, C) will stay in the lower stable state branch, leading to $\mathbb{P}_a$-status. The size of the bi-stability window ($W_G = [G^m, G^M]$) depends on other parameters and may even disappear for some parameter sets.

Fig 7A shows how main variables (C, I) in the system respond to the slowly increasing TGF-β level (G). The solution $C(t)$ (solid red line) initially follows the $\mathbb{P}_a$-status along the lower branch of the bifurcation curve until the right knee point of the bifurcation curve and transits to the upper branch solution, leading to the $\mathbb{P}_t$-mode. This trajectory of the solutions (C, I) along G is illustrated in Fig 7C. This illustrates that when G is increasing from a low value, the system will stay longer in the $\mathbb{P}_a$-phase. On the other hand, when G is slowly decreased from a high value, the solution $C(t)$ follows the upper branch of the bifurcation curve in Fig 6 until the left knee point and drops down to the lower branch, staying longer in the $\mathbb{P}_t$-phase

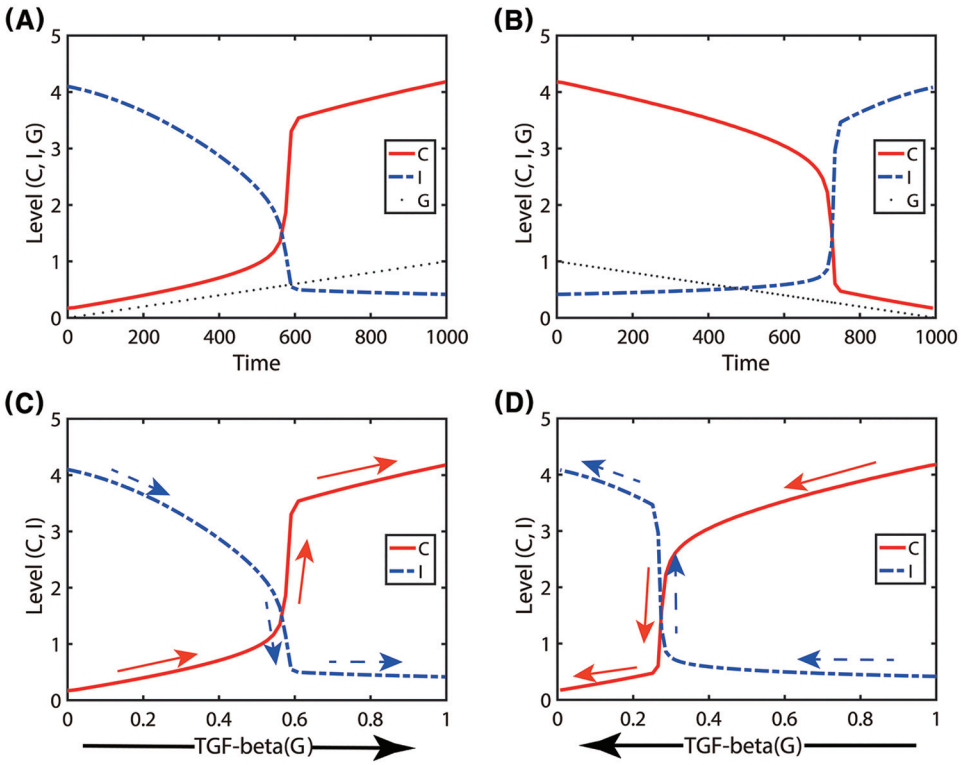

Fig 7. Immune response of TANs to increasing or decreasing TGF-β. (A, B) Time courses of the N2 (C, red solid curve) and N1 (I, blue dashed curve) levels as the TGF-β level (G; black dotted line) is slowly increased (from 0 to 1.0 in (A)) and slowly decreased (from 1.0 to 0.1 in (B)), respectively. (C, D) Change of C and I as a function of G corresponding to (A, B), respectively. Arrows indicate the moving direction of the solutions. $S = 0.2$. Other parameters are given in Table 2.

https://doi.org/10.1371/journal.pone.0211041.g007

including the bistability region W_G (Fig 6). The corresponding trajectory of the solutions (C, I) along G is shown in Fig 7D.

In Fig 8, we test the effect of fluctuating TGF-β on tumor growth. A time-dependent TGF-β level was assigned for a periodic supply of TGF-β in tumor microenvironment as follows (Fig 8A):

$$G(t) = \begin{cases} 0.002t + 0.2 & \text{if } 0 < t < 250 \\ -0.002(t - 250) + 0.7 & \text{if } 250 \leq t < 500 \\ 0.002(t - 500) + 0.2 & \text{if } 500 \leq t < 750 \\ -0.002(t - 750) + 0.7 & \text{if } 750 \leq t < 1000. \end{cases}$$

In response to the initial increasing TGF-β level, the trajectory of the solution $C(t)$ follows the lower branches of the hysteresis bifurcation loop (thick gray curve) and jumps to the upper branch (Fig 8B). However, a decrease in G around $t = 250$ switches the moving direction of the solution and it follows the upper branch in the bi-stability region until it jumps down to the lower branch near the left knee of the hysteresis curve. This flow of the solution ($G(t)$, $C(t)$) was marked in red arrows with initial position on the left lower corner (Fig 8B). The blue dashed curve and blue arrows represent the solution ($G(t)$, $I(t)$) and its flow, respectively, in the opposite side (Fig 8B). The detailed time courses of solutions ($C(t)$, $I(t)$) in response to the

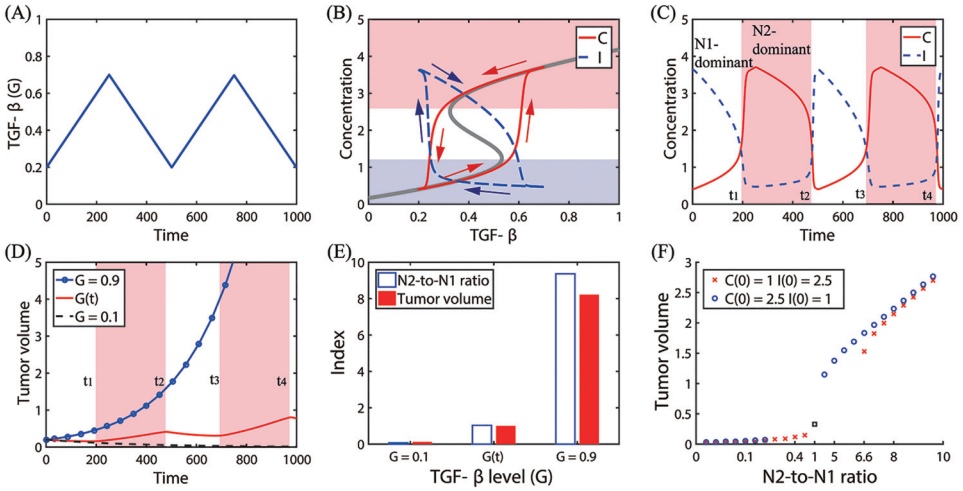

Fig 8. Effect of fluctuating TGF-β on tumor growth. (A) A time-dependent TGF-β level was assigned for a periodic supply of TGF-β in tumor microenvironment. (B) Trajectories of solutions (($G(t)$, $C(t)$) and ($G(t)$, $I(t)$)) in response to TGF-β in (A). The thick gray curve represents the upper and lower branches of steady states ($C - G$ hysteresis bifurcation loop in Fig 6). Red and blue arrows = solution flow direction of C and I, respectively. (C) Time courses of concentrations of C and I in response to periodic G input in (A). The N2-dominant $\mathbb{P}_t$-regions were shaded in pink. (D) Time courses of tumor volumes in response to a fixed ($G = 0.9$ (blue circle); $G = 0.1$ (dashed)) and fluctuating TGF-β level. Fluctuating TGF-β levels induce transitions between N1- and N2-dominant phenotypes, leading to transient tumor growth at the transition times (t_1, t_2, t_3, t_4). (E) The N2-to-N1 ratio and tumor size for three TGF-β conditions in (D). (F) Positive correlations between the tumor volume and the N2-to-N1 ratio with two initial conditions ($C(0) = 1$, $I(0) = 2.5$ in red asterisk; $C(0) = 2.5$, $I(0) = 1$ in blue circle). Initial conditions in (A-E): $C(0) = 0.4$, $I(0) = 3.6$, $G(0) = 0.2$, $T(0) = 0.2$. Other parameters are given in Table 2.

https://doi.org/10.1371/journal.pone.0211041.g008

periodic G input are shown in Fig 8C. The specific N1/N2 phenotypic transitions occur at time $t = t_1, t_2, t_3, t_4$. For example, the initial N1-dominant $\mathbb{P}_a$-status (white region in Fig 8C) switches to a N2-dominant $\mathbb{P}_t$-mode (pink region in Fig 8C) in the tumor microenvironment at time $t = t_1$ due to increasing TGF-β levels. The TAN phenotypic ratio, described by $\frac{C}{K+\gamma_1 I}$ in the second term of Eq (7), and N1 TAN immunity on tumor cells, described by δIT in the third term of Eq (7), determine either promotion or suppression of tumor growth in the model. Fig 8D shows time courses of tumor volumes in response to either fixed or varying TGF-β: (i) high TGF-β ($G = 0.9$, blue circle), (ii) low TGF-β ($G = 0.1$, dashed), and (iii) fluctuating TGF-β levels given in Fig 8A. The high TGF-β level induces N2-dominant $\mathbb{P}_t$-phase (Fig 5C), therefore, leading to N2-mediated, faster tumor growth (blue circle). When G is low, the system induces the N1-dominant $\mathbb{P}_a$ microenvironment (Fig 5A), resulting in N1-mediated, slower tumor growth (black dashed). On the other hand, fluctuating TGF-β induces alternating transitions between $\mathbb{P}_a$ (white region) and $\mathbb{P}_t$ (pink region) phases at $t = t_1, t_2, t_3, t_4$ (Fig 8C), which induces slow (white band in Fig 8D) or fast (pink band in Fig 8D) tumor growth in $\mathbb{P}_a$ and $\mathbb{P}_t$-regions, respectively, and eventually leads to an intermediate tumor volume at final time (Fig 8D). These results are in good agreement with experimental observations where N1 TANs significantly reduced the size of a tumor relative to N2 TANs [8]. The N2-to-N1 ratio (N21R) index and tumor volume corresponding to these three cases are shown in Fig 8E. An increase in the TGF-β level leads to an increase in the N2-to-N1 ratio, which in turn increase the tumor size. In Fig 8F, we investigate the correlation between N21R and the tumor size. The tumor volume and N21R were calculated from tumor and TAN populations in response to various TGF-β stimuli ($G = 0 - 0.9$) with two different initial conditions: $C(0) = 1$, $I(0) = 2.5$ in red asterisk; $C(0) = 2.5$, $I(0) = 1$ in blue circle. The case of the fluctuating $G(t)$ was marked in black square. As N21R is increased, the tumour volume is increased, leading to a positive

correlation between N21R and the tumor size. The neutrophil-to-lymphocyte ratio (NLR) has been highly associated with cancer progression [69, 70], becoming biomarkers for various cancers including non-small-cell lung cancer [71, 72] and cervical cancer [73]. In our simulation, N21R is equivalent to NLR and may be suggested to be a prognostic factor.

See S1 Appendix for analysis of the model. We investigated effects of N1 immunity (δ) on cancer cell killing. Depending on various values of δ, the killing rate of cancer cells by N1 TANs, time courses of tumor volume in response to fluctuating TGF-β may show different patterns: monotonic increase, monotonic decrease, or alternation between growth and shrinkage.

Dynamic transition to N1-dominant TANs by normalizing the complex immune system

In Fig 9A, we show the sensitivity of G-dependent N2 states (C^s) to changes in inhibition strength of the N2 module by the N1 module (α = 0.5, 1.5, 2.2, 6.0). The corresponding N1 states (I^s) are shown in Fig 9B. As α is increased, the bifurcation curve (C^s, G) shifts to the right. This increase in α also moves the bi-stability window (W_G) to the right and leads to a decrease in the size of the window ($|W_G|$). This indicates that the probability of switching to the anti-tumorigenic phase ($\mathbb{P}_a$) is increased when α is increased. For example, the immune response is already in the $\mathbb{P}_a$-phase ($C < C^{th}$, $I > I^{th}$) when G = 0.6 in the case of the higher α

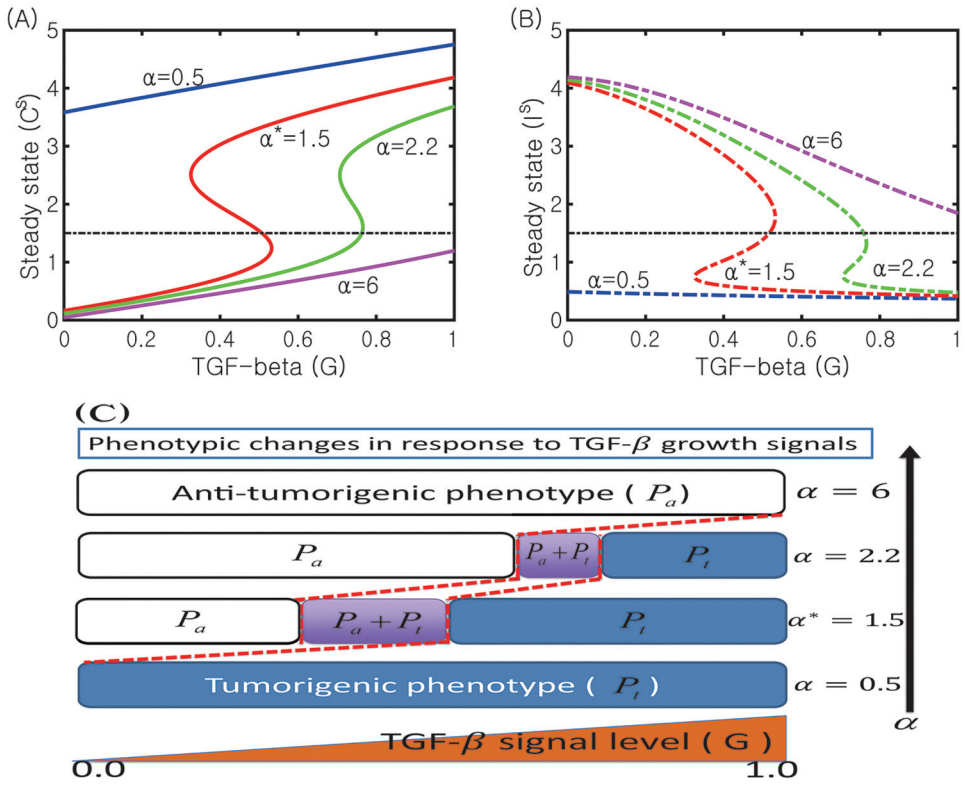

Fig 9. Transition to the N1-dominant environment by increasing α. (A, B) Bifurcation curves $G - C$ (C^s in (A)) and $G - I$ (I^s in (B)) for various N2 inhibition strengths (α = 0.5, 1.5, 2.2, 6.0). (C) The corresponding phenotypic switches between tumorigenic and anti-tumorigenic phases when α is varied. Other parameters are fixed as in Table 2. The base case (α^* = 1.5) was marked in star (*).

https://doi.org/10.1371/journal.pone.0211041.g009

value ($\alpha = 2.2$; green curve in Fig 9A) while it is still in the $\mathbb{P}_t$ phase ($C > C^{th}$, $I < I^{th}$) in the base case ($\alpha^* = 1.5$; red line in Fig 9A). On the other hand, the immune system would initiate the tumor-favoring progress even under low TGF-β conditions when α is decreased. For example, the system would be in the $\mathbb{P}_t$-phase for a low TGF-β signal ($G = 0.1$) when α is lowered ($\alpha = 0.5$; blue curve in Fig 9A) while it should be in the $\mathbb{P}_a$-phase in the base case ($\alpha^* = 1.5$). We recall that, for the base case ($\alpha^* = 1.5$), the existence of the bi-stability regime W_G illustrates that the TGF-β signal can regulate the forward transition from the $\mathbb{P}_a$-state to the $\mathbb{P}_t$-state and the recurrent process from the $\mathbb{P}_t$-state to the $\mathbb{P}_a$-state. However, when the N2 activity is highly enhanced with the decreased inhibition signal from the N1 complex (a decrease in α), the TGF-β signal may regulate only forward transition from the $\mathbb{P}_a$-state to the $\mathbb{P}_t$-state (one way switch) and a monotonic decrease in TGF-β signals does not push the immune system to the anti-tumorigenic phase. The phenotypic changes between $\mathbb{P}_a$- and $\mathbb{P}_t$-states for increased or decreased α are illustrated in Fig 9C. This mechanism of low α's therefore provides a way of keeping the immune system in a tumorigenic phase. Functional plasticity associated with a decrease in α induces a critical immunosuppressive switch to promote aggressive tumor growth and cancer progression [35, 74].

In Fig 10 we show the effect of the inhibition strength of N1 activities by the N2 module ($\beta = 0.1, 0.7, 1.0^*, 6.0$) on the dynamics of the core control system. As β is increased, the bifurcation curves (G, C) shift to the left (Fig 10A). In contrast to the case of changes in α in Fig 9, this increase in β reverses its shifting direction *i.e.,* it moves the bi-stability window (W_G) to the left and leads to an increase in the size of the window (W_G) despite disappearance of the

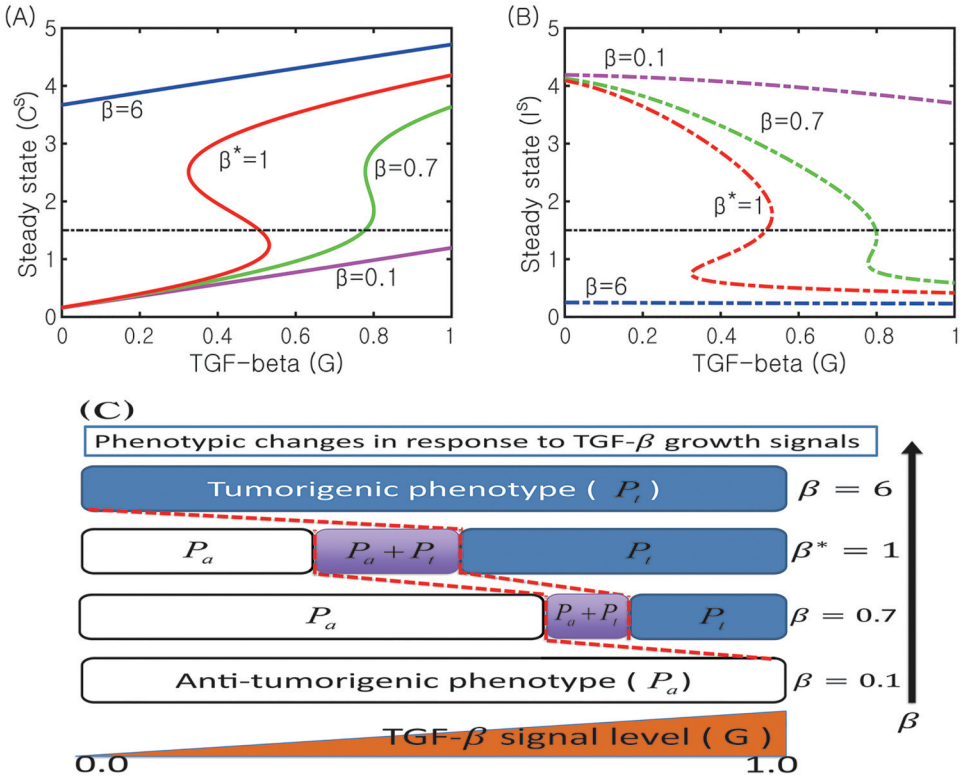

Fig 10. Effect of the inhibition parameter (β) on the transitions between N1 and N2 system. (A, B) Bifurcation curves $G - C$ (C^s in (A)) and $G - I$ (I^s in (B)) for for various N1 inhibition strengths ($\beta = 0.1, 0.7, 1.0^*, 6.0$). (C) The corresponding phenotypic switches between tumorigenic and anti-tumorigenic phases when β is varied. Other parameters are fixed as in Table 2. The base case ($\beta^* = 1.0$) was marked in star (*).

https://doi.org/10.1371/journal.pone.0211041.g010

bistable switch for larger β. Thus, an increase in β induces transient changes from a bistable- to a one-way-switch and to a mono-stability. This indicates that the probability of switching to the tumorigenic phase ($\mathbb{P}_t$) is increased in response to fluctuating TGF-β levels ($0 \leq G \leq 1.0$) when β is increased. For example, the immune system is already in the tumorigenic phase ($\mathbb{P}_t$; $C > C^{th}$, $I < I^{th}$) in response to $G = 0.12$ in the case of higher β's (for example, $\beta = 6.0$; blue curve in Fig 10A) while it should still be in the anti-tumorigenic phase ($\mathbb{P}_a$; $C < C^{th}$, $I > I^{th}$) in the base case ($\beta^* = 1.0$; red line in Fig 10A). On the other hand, the immune system would activate the anti-tumorigenic machinery even under high TGF-β signal conditions when β is decreased. For example, the system would increase probability of switching to the anti-tumorigenic phase by lowering N2 levels for a high TGF-β level ($G = 1.0$) when β is lowered ($\beta = 0.1$; cyan curve in Fig 10A) while it should be in the tumorigenic phase in the base case ($\beta^* = 1.0$). While a decrease in β reduces the size of the bi-stability window ($|W_G|$), an increase in β reduces the size of the one-way switch window. When N2 activities are highly enhanced with the increased inhibition signal of the N1 module by the N2 complex (an increase in β) due to mutual antagonism between N2 and N1 modules, TGF-β signals may also regulate only forward transition from $\mathbb{P}_a$-state to $\mathbb{P}_t$-state (one way switch) and a monotone decrease in TGF-β signals does not push the immune system to the anti-tumorigenic phase. Therefore, this β-induced mechanism has a similar effect on keeping high N2 activities as that of a decrease in α, providing a way of keeping the immune system in a tumorigenic phase.

Therefore, these results provide a scientific basis for targeting suppressive effect of N2 TANs by normalizing immune activities (increase in α or decrease in β) within the tumor microenvironment or keeping a favorable balance of the N1/N2 TAN's properties toward N1 TANs [35]. For example, blood normalization was suggested to be an alternative way of creating anti-tumor TAN microenvironment [75, 76].

Role of IFN-β signaling in regulation of the transition between N1- and N2-dominant system

In Fig 11, we investigate the role of the IFN-β signaling pathway in the phenotypic balance of N2 and N1 complexes for various TGF-β levels ($G = 0.1, 0.5, 0.65$). When G is low, the system induces a bi-stable system for low IFN-β levels and N1-dominant phenotypes in response to intermediate and high IFN-β levels (Fig 11A). Therefore, the system is quite sensitive to relatively low IFN-β stimuli to induce the anti-tumor microenvironment. When G is increased to $G = 0.5$, the bistability window (W_s) in Fig 11A moves to the right and the system now can generate tumorigenic, bi-stable, and anti-tumorigenic status in response to low, intermediate, and high IFN-β levels, respectively. Therefore, the relative balance between TGF-β and IFN-β signaling determines the phenotypic preference (Fig 11B). On the other hand, in the presence of high levels of TGF-β ($G = 0.65$; Fig 11C), the bistability window disappears and the probability of inducing a N1-dominant microenvironment is decreased, shifting the balance toward the high N2-to-N1 ratio. Fig 11D summarizes the phenotypic representation of the system in response to various TGF-β and IFN-β stimuli. The majority of the bi-stable region resides in the lower left corner of the $G - S$ plane. Therefore, the biochemical fluctuation of both TGF-β and IFN-β levels in the lower regime is likely to generate a selection process of either promoting or suppressing tumor growth based on the initial distribution and phenotypic status of TANs in tumor microenvironment.

Sensitivity analysis

In the model developed in this paper, there are parameters for which no experimental data are known and they may affect the simulation results. We take all parameters in the model (r, K,

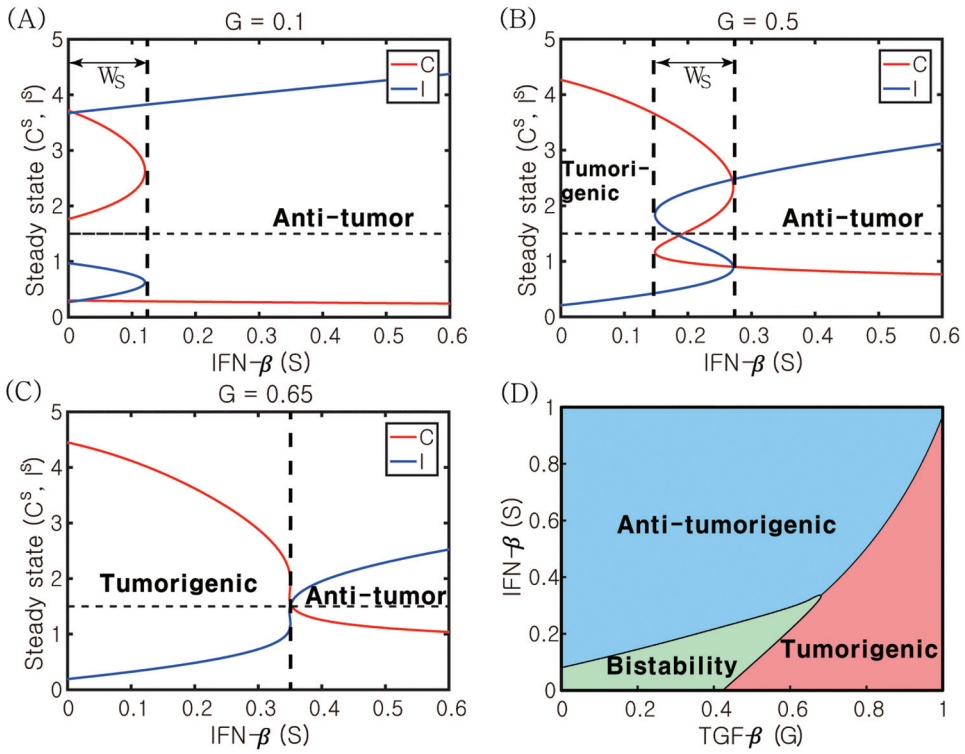

Fig 11. Dynamic change in response to the IFN-β signal. (A-C) Activities of N2- and N1-modules in response to IFN-β levels (S) when the TGF-β level is low ($G = 0.1$ in (A)), intermediate ($G = 0.5$ in (B)), and high ($G = 0.65$ in (C)). When the TGF-β level is low or intermediate, there exists a bi-stable window ($W_S = \{S \in [0, 1]: S^m \leq S \leq S^M\}$) where both $\mathbb{P}_t$ and $\mathbb{P}_a$ coexist. (D) For a constant IFN-β signaling, the system transits from $\mathbb{P}_a$- to $\mathbb{P}_t$-modes as the TGF-β level is increased. On the other hand, for a fixed TGF-β level, an increase in S induces a transition from $\mathbb{P}_t$-favoring mode to the $\mathbb{P}_a$-status. Other parameters are given in Table 2.

https://doi.org/10.1371/journal.pone.0211041.g011

γ_1, T_0, λ, δ, G, S, k_1, k_2, k_3, k_4, α, β, and μ) for sensitivity analysis. We investigated the sensitivity of the activities of N2 and N1 modules at $t = 10, 100, 200$ to these parameters. We have chosen a range for each of these parameters and divided each range into 10,000 intervals of uniform length. For each of the fifteen parameters of interest, a partial rank correlation coefficient (PRCC) value is calculated. PRCC values range between -1 and 1 with the sign determining whether an increase in the parameter value will decrease (-) or increase (+) activities of the N2 and N1 complex, and tumor size at a given time. The sensitivity analysis to be described below was carried out using the method from [77] and Matlab files available from the website of Denise Kirschner's Lab: http://malthus.micro.med.umich.edu/lab/usadata/.

Fig 12 shows the sensitivity analysis results for the N2 level and N1 activity, and tumor volume at $t = 10, 100, 200$ for Eqs (5)–(7) *i.e.,* we compute PRCC values for C, I, T at time $t = 10, 100, 200$. We calculate PRCC values and associated p-value for fifteen perturbed parameters (r, K, γ_1, T_0, δ, λ, G, S, k_1, k_2, k_3, k_4, α, β, μ). We conclude that the activity of the N2 complex at $t = 200$ is positively correlated to the parameters λ, G, μ but is very little correlated (and thus not sensitive) to r, K, γ_1, T_0, α, β, k_1, k_2, k_3, k_4, S. Thus, in particular, the N2 level will increase significantly if the TGF-β signal is increased. Due to mutual antagonism between N1- and N2-dominant system, it is expected to see opposite correlations between N1 activity and those parameters. Indeed, the N1-dominant system is positively correlated to the parameters k_2, S but is negatively correlated to the parameters G, β, k_4, μ, *i.e.,* there would be significant reduction in the N1 expression level if the TGF-β signaling strength is increased. The tumor volume

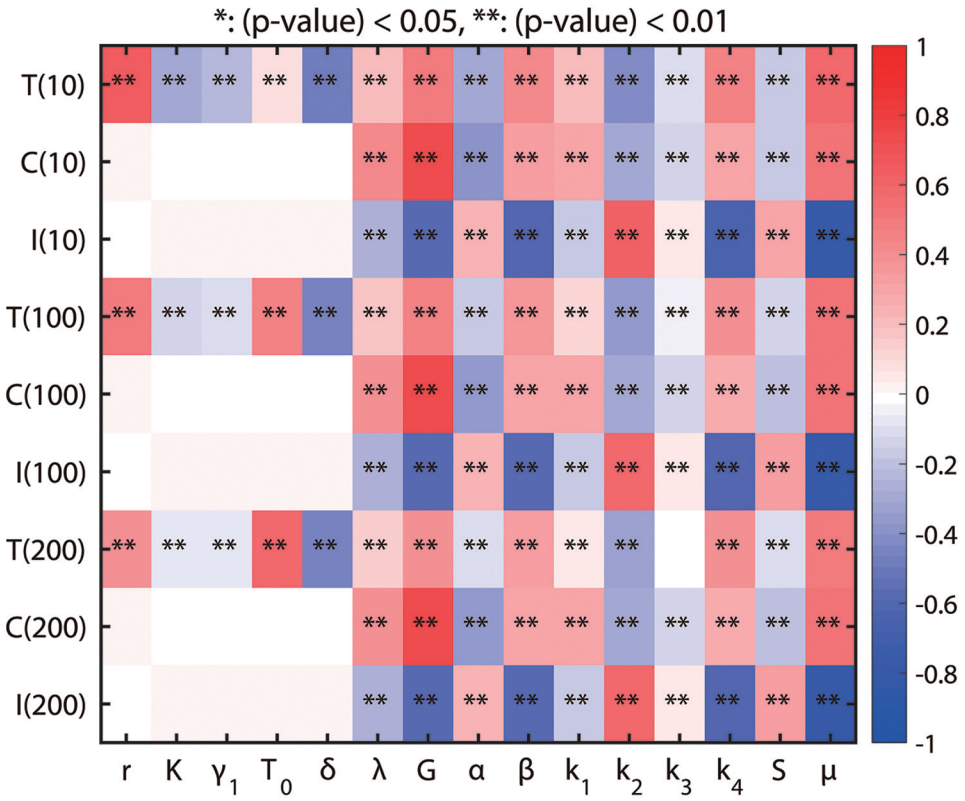

Fig 12. Sensitivity analysis: General Latin Hypercube Sampling (LHS) scheme and partial rank Correlation Coefficient (PRCC) performed on the model. The colors in each sub box indicates PRCC values of the N2 level and N1 activity for model parameters (r, K, γ_1, T_0, δ, λ, G, S, k_1, k_2, k_3, k_4, α, β, μ) at t = 10, 100, 200. The analysis was carried out using the method of [77] with sample size 10000.

https://doi.org/10.1371/journal.pone.0211041.g012

is positively correlated to the growth rate (r) and carrying capacity (T_0) but is negatively correlated to the tumor killing rate by N1 TANs (δ).

Therapeutic approaches: Blocking the N2-dominant system by TGF-β inhibitors

In Fig 13 we investigate the anti-tumor effect of a TGF-β inhibitor on tumor growth. We introduce new variables: concentration of TGF-β (G), instead of a parameter, and TGF-β inhibitor concentration (L) whose dynamics are described as follows:

$$\frac{dG}{dt} = G_s - \mu_G G - \gamma_L L G, \tag{8}$$

$$\frac{dL}{dt} = \sum_{i=1}^{N_L} L_s J_{[t_i, t_i+h_d]} - \mu_L L. \tag{9}$$

Here, G_s is the constant source of TGF-β, μ_G is the decay rate of TGF-β, γ_L is the degradation rate of TGF-β by its inhibitor, L_s is the external periodic source of the TGF-β inhibitor on the time intervals $[t_i, t_i + h_d]$, $i = 1, \ldots, N_l$ with the duration h_d and the period τ_L ($= t_{i+1} - t_i$, $i = 1, \ldots, N_L - 1$; $h_d < \tau_L$) between those intervals, N_L is the number of injections, $J[\cdot]$ is the indicator function (giving 1 and 0 on the given condition), μ_L is the decay rate of the TGF-β

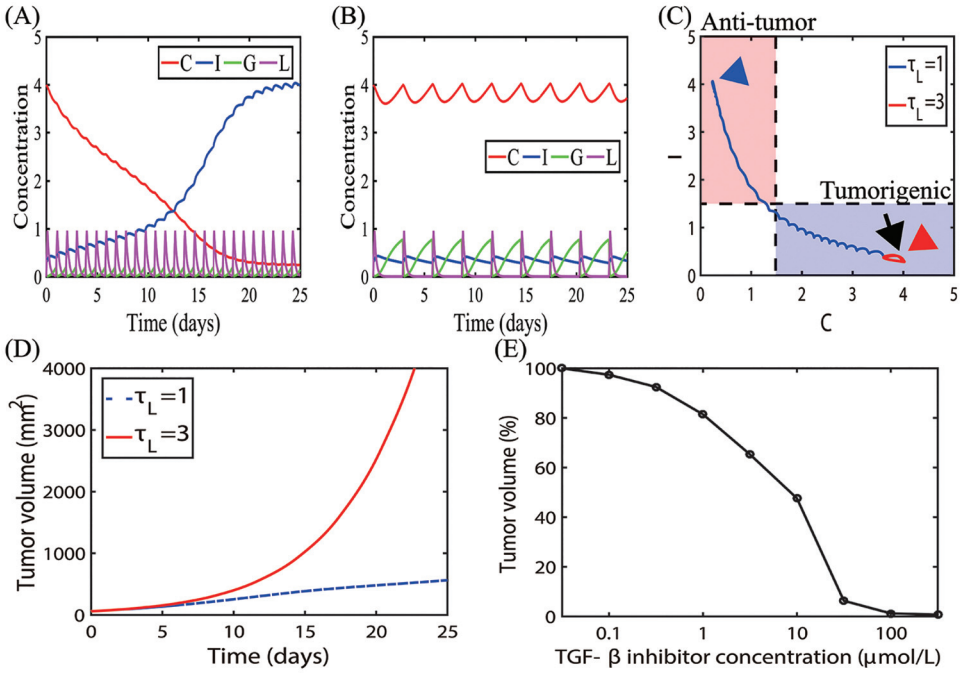

Fig 13. Therapeutic effect of TGF-β inhibitor injection. (A, B) Time courses of activity levels of the N2 complex (C) and N1 complex (I), and concentrations of TGF-β (G) and TGF-β inhibitor (L) in response to a periodic injection of the TGF-β inhibitor with periods $\tau_L = 1$ (A) and $\tau_L = 3$ (B), respectively. (C) Dynamics of the core N1-N2 system in response to the frequent ($\tau_L = 1$ in (A)) and less frequent ($\tau_L = 3$ in (B)) injections of the TGF-β inhibitor in the $C - I$ plane. (D) Time courses of tumor volume for two different injection protocols in (A, B). (E) Tumor volume (%) at final time ($t = 25$ *days*) in response to various TGF-β inhibitor levels (0, 0.02, 0.1, 0.3, 1.0, 3.0, 10, 20, 100 $\mu mol/L$). Initial conditions: $C(0) = 4.0$, $I(0) = 0.3$, $G(0) = 0$, $L(0) = 0$. Initial injection time: $t_1 = 0$. All other parameters are fixed as in Table 2.

https://doi.org/10.1371/journal.pone.0211041.g013

inhibitor. Eqs (8) and (9) then are coupled with the original Eqs (5)–(7) to investigate the effect of TGF-β inhibitors on the transition behaviors between N1 and N2 phenotypes. In Fig 13(A) and 13(B), the dynamic system shows different mode changes as the TGF-β inhibitor was injected at the different periods ($\tau_L = 1, 3$). A frequent injection of the inhibitor ($\tau_L = 1$ in Fig 13A) induces a decrease in the TGF-β level ($G < 0.4$), resulting in the transition from the initial tumorigenic condition (black arrow in Fig 13C) to the anti-tumorigenic mode (blue arrowhead in Fig 13C). On the other hand, the TGF-β level still stays in the upper stable branch (Fig 6) in response to a less frequent injection schedule ($\tau_L = 3$ in Fig 13B), keeping the system in the tumorigenic phase (red arrowhead in Fig 13C). These different cellular compositions in N1- or N2-dominant tumor microenvironment result in fast or slow tumor growth: slow and fast tumor growth in response to frequent ($\tau_L = 1$) and less frequent ($\tau_L = 3$) injection schedules, respectively (Fig 13D). Fig 13E shows the normalized tumor volume at final time ($t = 25$ *days*) for various TGF-β inhibitor levels ($L_0 = 0 - 100$ $\mu mol/L$). As the loading dose is decreased, the anti-tumor efficacy is significantly decreased especially when its concentration is less than 10 $\mu mol/L$. These results are in good agreement with experimental data [38]. Serizawa *et al.* [38] found that gefitinib, a TGF-β inhibitor, can effectively kill non-small-cell lung cancer cells, PC-9 (cell lines without erlotinib, an EGFR inhibitor) and PC-9ER1/PC-9ER4 (cell lines with resistance to erlotinib) in *in vitro* experiments [38]. While the overall cell viabilities in these cell lines were significantly decreased in response to the increasing concentrations of gefitinib, the anti-tumor efficacy in low dose of gefitinib ($\sim 0.1 \mu mol/L$) was higher and sensitive in PC-9 cell lines in the response curve. This implies that the higher dose TGF-β

inhibitor needs to be injected into the tumor in order to maintain the same level of anti-tumor efficacy in the tumor microenvironment.

Therapeutic strategies by IFN-β injection

We investigate the effect of normalizing immune activities on tumor growth by injecting IFN-β. We consider the following conventional equations for time-dependent IFN-β administration:

$$\frac{dS}{dt} = \sum_{i=1}^{N_s} S_s J_{[t_i, t_i+h_s]} - \mu_S S \tag{10}$$

where S_s is the injection dose of IFN-β, $J(\cdot)$ is the indicator function. The IFN-β is injected over the time interval $[t_i, t_i + h_s]$, $i = 1, \ldots, N_s$ for the time duration h_s and a period τ_s ($= t_{i+1} - t_i$, $i = 1, \ldots, N_s - 1$), N_s is the number of the IFN-β injections.

Fig 14A shows the time courses of N2 levels (C), N1 activity (I), and IFN-β level (S) in response to intratumoral injections of IFN-β. Fig 14B shows the corresponding trajectory of the solution ($C(t)$, $I(t)$) in the $C - I$ plane. Starting from an initial condition in the tumorigenic phase (black arrow in Fig 14B), the N2-dominant system responds to the injected IFN-β in a periodic fashion and slowly transits to the N1-dominant system (pink box in Fig 14B) by decreasing the N2 level and increasing N1 activity (blue arrowhead). Fig 14C shows time courses of tumor volume (mm^2) in the absence (PBS; red solid curve, $S_s = 0$) and presence (blue dashed curve, $S_s = 35$) of intratumoral injection of IFN-β. IFN-β treatment significantly reduces the tumor size through repressing the N2-suppressing immune microenvironment (Fig 14B), which is in good agreement with experimental data. Note that even though the (C, I) returned back to the tumorigenic phase (blue arrowhead in Fig 14B) after the last IFN-β injection on day 9 (Fig 14A), the overall tumor growth is still very slow due to the earlier suppression of the N1-dominant environment, thus normalizing the immune activities against the tumor. The empty circles and triangles in Fig 14C represent experimental results for the LLC1 tumor cell line implanted in C57BL/6 mice in controls (PBS; empty circle) and after IFN-β injection (triangles) cases, respectively [36]. In Fig 14D, we show the dose-response curve of IFN-β at day 25 after a periodic intratumoral injection of IFN-β when $G = 0.4$. IFN-β therapy in combination with other anti-tumor drugs [36] has been suggested to be effective in reducing tumor growth [22–25] and stimulating the anti-tumor immune response [37]. Fig 14E shows the average N1-Tcell levels over the time interval [0–12 *days*] in the absence of IFN-β (PBS; white bar) and in response to various IFN-β doses (35,70,100 $\mu mol/L$; black bars). The corresponding average N2 populations are shown in Fig 14F. In experimental studies [28], the relative population of tumor-infiltrating CD8 T cells were significantly increased in tumor microenvironment in response to IFN-β treatment but the Treg population was reduced in non-small cell lung cancer. The model predicts a significant increase in the immune activities (Fig 14E) and dramatic decrease in Treg populations, which is consistent with the experimental results [28].

In Fig 15A, we show anti-tumor efficacy for various dose schedules and injection doses of IFN-β. For a fixed IFN-β dose, the low (or high) dosing frequency induces N2-dominant (or N1-dominant) tumor microenvironment and thus faster (or slower) tumor growth. For a fixed injection frequency, the system transits from the N2-dominant phase to the N1-dominant phase, thus slower tumor growth, as the injection dose amount (S_s) is increased as shown in Fig 14. The mathematical model predicts that the larger injection period (τ_s) and smaller dose (S_s) would result in the N2-mediated, faster tumor growth while the frequent injection schedule and larger doses would lead to the phenotypic switch to the N1-dominant microenvironment

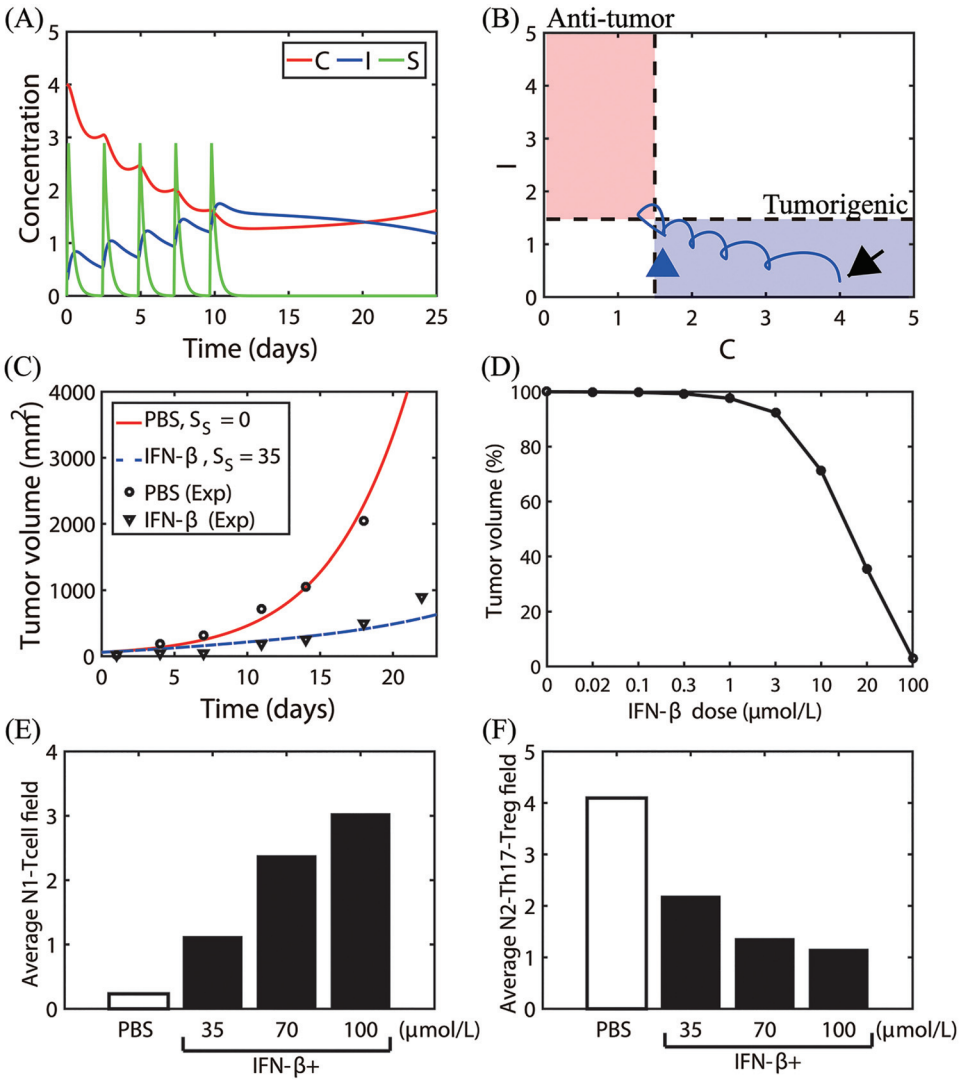

Fig 14. Therapeutic effect of IFN-β on tumor growth. (A) Time courses of the N2 complex level (C), N1 complex activity (I), and concentration of IFN-β (S) in response to a periodic injection of IFN-β on 0, 3, 5, 7, 9 *days*. (B) Dynamics of the core N1-N2 system corresponding to (A) in the $C - I$ plane. Black arrow = initial position, blue arrowhead = terminal point at $t = 25$ *days*. (C) Time courses of tumor volume in control (PBS) and IFN-β^+ cases: Control (PBS) from the model (red solid line, $S_s = 0$), IFN-β injection case from the model (blue dashed line, $S_s = 35$), control (PBS) from experiments (empty circle), IFN-β injection case from experiments (triangle). (D) Tumor volume (%) at final time ($t = 25$ *days*) in response to various IFN-β injection levels ($S_s = 0, 0.02, 0.1, 0.3, 1.0, 3.0, 10, 20, 100$ $\mu mol/L$). (E, F) Tumor-infiltrating CD8 T cells and Tregs. Average field of N1-Tcell (E) and N2-Th17-Tregs (F) over the time interval [0–12 *days*], in the absence (PBS) and presence of IFN-β injections (35,70,100 $\mu mol/L$). Initial conditions: $C(0) = 4.0$, $I(0) = 0.3$, $S(0) = 0$. Initial injection time: $t_1 = 0$. Parameters used: $G = 0.4$. All other parameters are fixed as in Table 2.

https://doi.org/10.1371/journal.pone.0211041.g014

and the greater anti-tumor efficacy. Unfortunately, IFN therapy has been shown to be associated with side effects and significant toxicity in cancer, including neuropsychiatric, constitutional, hepatic, and hematologic effects [78], as well as in multiple sclerosis [79]. Therefore, clinicians would want to optimize the overall administration schedule in order to minimize the dose amount while still avoiding high dose therapy and maintaining sustainable clinical results. In other words, the dose level needs to be minimized in order to avoid drug complication region in Fig 15B. On the other hand, too frequent injections are not desirable due to an

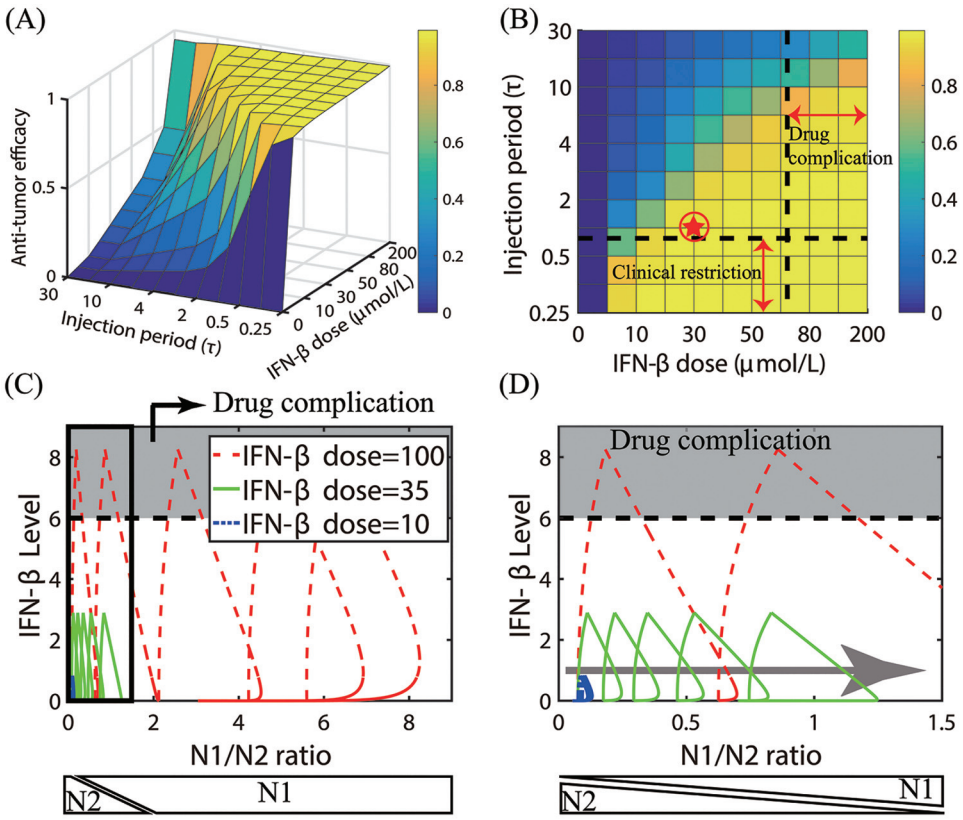

Fig 15. Optimal anti-tumor strategies of IFN-β injection. (A) Anti-tumor efficacy for various dose schedules (τ_s = 0.25, 0.33, 0.5, 1, 2, 3, 4, 5, 10, 15, 30 *days*) and injection doses of IFN-β (5, 10, 20, 30, 40, 50, 60, 80, 100, 200 $\mu mol/L$). (B) Illustration of anti-tumor efficacy for various schedules in (A) with practical restrictions at a clinic. The optimal dose and schedule are obtained for an intermediate IFN-β dose and an injection schedule without drug complication and under clinical restrictions (100 $\mu mol/L$, τ_s = 1 *day*; red asterisk). (C) Trajectories of solutions ($\Gamma(t)$, $S(t)$) in the IFN-β-Γ plane in response to low (10 $\mu mol/L$, blue dashed line), intermediate (35 $\mu mol/L$, green solid line), and high (100 $\mu mol/L$, red dashed line) doses of IFN-β every day (τ_s = 1 *day*). Here, $\Gamma(t)(= I(t)/C(t))$ and $S(t)$ are the N1/N2 ratio and IFN-β concentration, respectively, at time t. (D) Enlarged figure from a subpanel (black box on the left) in (C). As the injection strength is increased (10→35→100), the trajectory transits to the N1-dominant system (gray arrow). However, the high dose IFN-β may lead to drug complications or extensive associated toxicity (gray zone on the top) [83–86]. N1 and N2 phenotypes on the bottom of panels (C, D) are determined from the N1/N2 ratio.

https://doi.org/10.1371/journal.pone.0211041.g015

increase in administrative costs at a clinic, *i.e.,* avoiding clinical restriction region in Fig 15B. In our simulations, the optimal treatment schedule can be obtained with an intermediate dose of 30 $\mu mol/L$ and τ_s = 1 *day* (red circled asterisk in Fig 15B) as explained below. In Fig 15C we show the trajectories of solutions ($\Gamma(t)$, $S(t)$) in the IFN-β-N1/N2 plane in response to the low (10 $\mu mol/L$, blue dashed line), intermediate (35 $\mu mol/L$, green solid line), and high (100 $\mu mol/L$, red dashed line) doses of IFN-β every day (τ_s = 1 *day*). Here, $\Gamma(t)(= I(t)/C(t))$ and $S(t)$ are the N1/N2 ratio and IFN-β concentration, respectively, at time t. An enlarged subpanel (black box on the left) in Fig 15C is shown in Fig 15D. As the injection strength is increased (10→35→100), the N1/N2 ratio is increased and the tumor microenvironment transits from N2- to the N1-dominant system (gray arrow), leading to better anti-tumor efficacy (Fig 15A). High doses of IFN-β were shown to suppress tumor cell proliferation and promote cell death in both *in vitro* and *in vivo* experiments [80–82]. However, a high IFN-β dose also increases IFN-β levels, leading to drug complications or extensive associated toxicity (gray zone on the top)

[83–86]. Therefore, the injection schedule should be designed to avoid the associated toxicity but still maximize the N1/N2 ratio for optimal clinical outcome.

Combination therapy

In this section, we investigate the effect of a combined therapy (TGF-β-inhibitor +IFN-β) therapy on tumor growth by solving Eqs (5)–(10). Fig 16A shows time courses of the activities of N2 (C) and N1 (I) modules, and concentrations of TGF-β (G), TGF-β inhibitor (L), and IFN-β (S) in response to a periodic injection of TGF-β inhibitor every day ($\tau_L = 1\ day$) and IFN-β on 0, 3, 5, 7, 9 days ($L_s = 8$, $S_s = 20$). Injections of both two drugs induce a decrease in C and increase in I, generating the N1-favoring microenvironment, thus suppressing tumor growth. When these drugs are administered more often ($\tau_L = 1\ day$, $\tau_s = 1\ day$), the system quickly switches from the N2-favoring system to the N1-dominant system even with lower doses ($L_s = 5$, $S_s = 15$; See Fig 16B). Fig 16C shows the trajectories of solutions ($C(t)$, $I(t)$) in response to control (PBS, red) and injections of IFN-β alone (blue), TGF-β inhibitor alone (TGF-β^-, green), and combination therapy (IFN-β + TGF-β inhibitor, black): $L_s = 8$, $S_s = 20$. While solutions in control (PBS) and single drug (either IFN-β or TGF-β inhibitor) stay in the tumorigenic phase (arrowheads (red, blue, green) in the blue box), the solution in the combination therapy (TGF-β inhibitor+IFN-β) moves to the anti-tumorigenic region (black arrowhead in the pink box). Thus, these dynamics illustrate how the combination therapy may induce the transition from the $\mathbb{P}_t$-phase to the $\mathbb{P}_a$-phase even when either TGF-β inhibitor or IFN-β

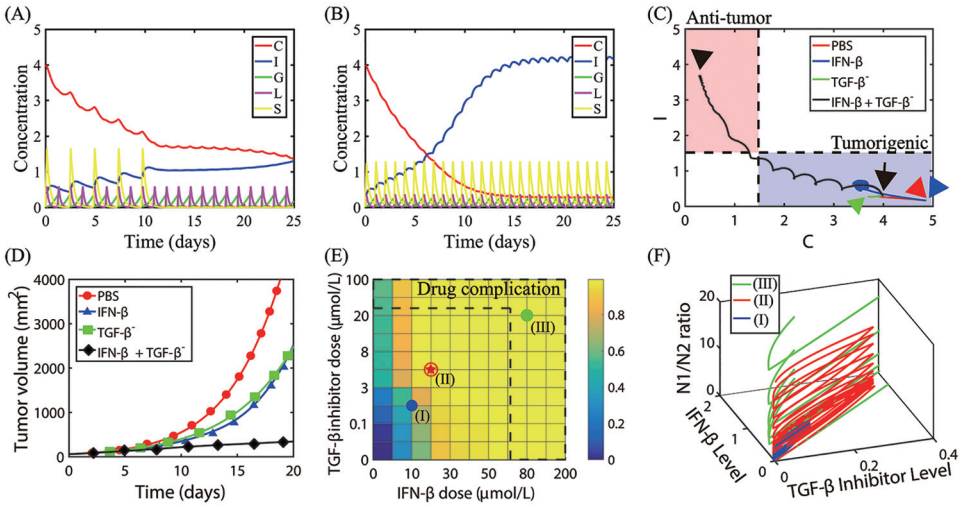

Fig 16. Therapeutic effect of a combination therapy (TGF-β inhibitor + IFN-β) on tumor growth. (A) Time courses of the N2 (C) and N1 complex (I) activity, and concentrations of TGF-β (G), TGF-β inhibitor (L), and IFN-β (S) in response to a periodic injection of TGF-β inhibitor every day ($\tau_L = 1\ day$) and IFN-β on 0, 3, 5, 7, 9 days. $L_s = 8$, $S_s = 20$. (B) Time courses of all variables (C, I, G, L, S) in response to a periodic injection of both TGF-β inhibitor and IFN-β every day. $L_s = 5$, $S_s = 15$. (C) Trajectories of solutions ($C(t)$, $I(t)$) in response to control (PBS, red) and injections of IFN-β only (blue), TGF-β inhibitor only (TGF-β^-, green), and combination therapy (IFN-β + TGF-β inhibitor, black). Black arrow = initial position, arrowheads = terminal points at $t = 25\ day$ for four cases. $L_s = 8$, $S_s = 20$. (D) Time courses of tumor volume corresponding to four cases in (C). The combination therapy leads to synergistic effect on killing tumor cells. (E) Anti-tumor efficacy of the combination therapy with various doses of IFN-β (0, 5, 10, 20, 30, 40, 50, 60, 80, 100, 200) and TGF-β inhibitor (0, 0.02, 0.1, 0.3, 3, 5, 8, 10, 20, 50, 100) at final time ($t = 25\ days$). The optimal dose schedule (marked in red asterisk) is obtained by avoiding drug complications and minimizing dose levels while maintaining the high anti-tumor efficacy. (F) Trajectories of solutions ($L(t)$, $S(t)$, $\Gamma(t)$) for the low (blue; (I) in (E)), intermediate (red; (II) in (E)), and high (green; (III) in (E)) doses of both TGF-β inhibitor and IFN-β. Here, $\Gamma(t) = I(t)/C(t)$ is the N1/N2 ratio. Initial conditions: $C(0) = 4.0$, $I(0) = 0.3$, $G(0) = 0$, $L(0) = 0$, $S(0) = 0$. Initial injection time: $t_1 = 0$. All other parameters are fixed as in Table 2.

https://doi.org/10.1371/journal.pone.0211041.g016

therapy transits the system to the $\mathbb{P}_t$-mode. Time courses of the tumor volume corresponding to four cases in Fig 16C are shown in Fig 16D. Thus, the combination therapy leads to synergistic tumor killing effects via switching to the $\mathbb{P}_a$-phase (Fig 16C). Fig 16E shows anti-tumor efficacy of the combination therapy with various doses of IFN-β and TGF-β inhibitor at final time ($t = 25$ *days*). For a fixed dose level of either IFN-β or TGF-β inhibitor, the anti-tumor efficacy is increased in general. However, high doses of either IFN-β [78, 85–87] or TGF-β inhibitor [88, 89] alone can induce toxicity, resistance and side effects. Therefore, careful dosing strategies need to be developed in order to efficiently deliver IFN-β to a tumor and maximize anti-tumor efficacy while minimizing critical, systemic side effects [90, 91]. Therefore, double high doses of those two drugs may not be desirable due to economic costs as well as serious side effects. It has been shown that high doses of TGF-β inhibitors may lead to poor response to the combined 5-fluorouracil and IFNα-2b therapy in hepatocellular carcinoma patients [92]. The optimal drug dose schedule (red asterisk) can be obtained by avoiding drug complications (dotted region on the upper and right sides) and minimizing dose levels of both drugs while maintaining the overall high anti-tumor efficacy. Fig 16F shows the trajectories of solutions ($L(t)$, $S(t)$, $\Gamma(t)$) for the low (blue; (I) in Fig 16E), intermediate (red; (II) in Fig 16E), and high (green; (III) in Fig 16E) doses of both TGF-β inhibitor and IFN-β. Here, $\Gamma(t) = I(t)/C(t)$ is the N1-to-N2 ratio. While the N1-to-N2 ratios in (II) and (III) are large, the N1-to-N2 ratio is small for low doses of IFN-β and TGF-β inhibitor (case (I)). Thus, the case (III) in Fig 16E is not desirable because of the high N1-to-N2 ratio.

Effect of time delays

We investigated the effect of time delays on regulation of phenotypic switches and tumor growth. We prescribe time delays in the suppression terms of the N2 and N1 complex. There are many cellular and molecular factors that may affect delayed processes of signaling pathways, apoptosis, and inhibition of neutrophils in the microenvironment [62, 93–96]. This may also be caused by partial blocking of signaling pathways of these TANs by drugs. Recall that the transition probability between $\mathbb{P}_t$ and $\mathbb{P}_a$-phases can be modified by the mutual inhibition strength of both N1 and N2 complex (α, β; Figs 9 and 10). Therefore, we modify Eqs (5) and (6) by introducing time delays in the inhibition terms as follows

$$\frac{dC}{dt} = \lambda_1 + G + \frac{k_1}{k_3^2 + \alpha[I(t-\Delta_1)]^2} - C(t), \tag{11}$$

$$\frac{dI}{dt} = S + \frac{k_2}{k_4^2 + \beta[C(t-\Delta_2)]^2} - \mu I(t), \tag{12}$$

where Δ_1, Δ_2 are the time delays in the inhibitory pathway of the N2 module and suppression of N1 module, respectively (See Fig 4B). Fig 17A shows concentrations of two main variables (C, I) in the absence (ODE, red) and presence (DDE, blue) of time delays $(\Delta_1, \Delta_2) = (1.0, 1.2)$ with initial condition: $T(0) = 0.2$, $C(0) = 1.2$, $I(0) = 0.5$. The corresponding trajectories of solutions ($C(t)$, $I(t)$) without (red dotted) and with (solid blue) time delays are shown in Fig 17B. Starting with the same initial condition (black arrow), the system adapts to changes in the microenvironment by inducing tumorigenic status (C high, I low; blue box) and anti-tumorigenic mode (C low, I high; pink box) in the absence and presence of time delays, respectively. This delay-induced $\mathbb{P}_a$ mode results in a decrease in the tumor size (Fig 17C). This illustrates that the time delays in suppressing N1 or N2 TANs may stimulate a homeostatic imbalance, resulting in either promotion or suppression of tumor growth. Fig 17D shows the normalized tumor volume at day 25 for various strengths of the two time delays (Δ_1, Δ_2). For a fixed Δ_1, as

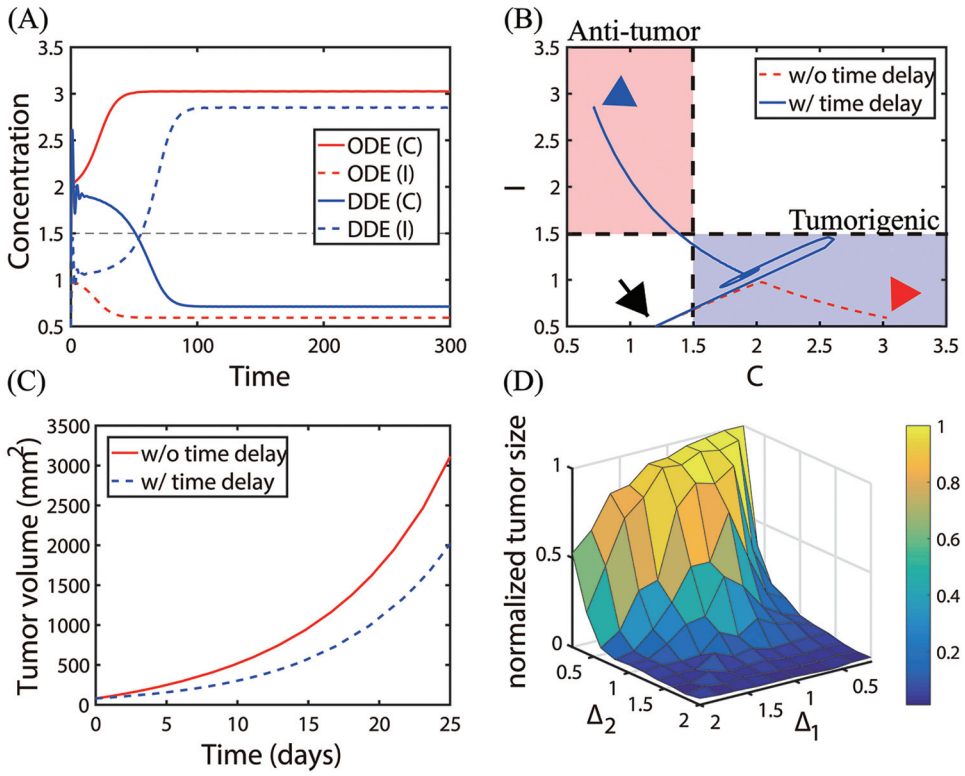

Fig 17. Dynamics of the system with time delays (Δ_1, Δ_2) in inhibition of TANs. (A) Time courses of concentrations of two main variables (C, I) in the absence (ODE, red) and presence (DDE, blue) of time delays ($\Delta_1 = 1.0$, $\Delta_2 = 1.2$). (B) Trajectories of solutions ($C(t)$, $I(t)$) in the $C - I$ plane corresponding to (A). Time delays can push the $\mathbb{P}_t$-phase to the $\mathbb{P}_a$-phase. (C) Time courses of the tumor volumes corresponding to (A, B). Time delays can slow down the tumor size by the N1 to N2 transition in (B). (D) Normalized tumor sizes for various strengths of the two time delays (Δ_1, Δ_2). Parameters: $S = 0.2$, $G = 0.4$. All other parameters are fixed as in Table 2. Initial condition: $T(0) = 0.2$, $C(0) = 1.2$, $I(0) = 0.5$.

https://doi.org/10.1371/journal.pone.0211041.g017

Δ_2 is increased, the inhibition strength of the N1 module is decreased and N1 TANs become a dominant phenotype, decreasing the tumor volume. For a fixed Δ_2, the tumor size is a nonlinear function of Δ_1, inducing a small tumor for either high or low Δ_1 but assuming the maximum tumor size for an intermediate Δ_1. These results illustrate the complex dynamics of the N1/N2 transitions and nonlinear tumor growth in the presence of time delays in mutual inhibitory properties.

Now, we investigate the effect of time delays in apoptosis of TANs by modifying Eqs (5) and (6) by introducing time delays in the decay term as follows

$$\frac{dC}{dt} = \lambda_1 + G + \frac{k_1}{k_3^2 + \alpha I^2} - C(t - \Delta_3), \tag{13}$$

$$\frac{dI}{dt} = S + \frac{k_2}{k_4^2 + \beta C^2} - \mu I(t - \Delta_4), \tag{14}$$

where Δ_3, Δ_4 are the time delays in apoptosis of N2 and N1 modules, respectively. Fig 18(A) and 18(B) show time courses of the N2- and N1-modules in the absence (ODE, red) and presence (DDE, blue) of time delays: $(\Delta_3, \Delta_4) = (1, 1)$ in (A), $(\Delta_3, \Delta_4) = (0.9, 1)$ in (B). Fig 18C shows trajectories of the corresponding solutions ($C(t)$, $I(t)$) in the $C - I$ plane. The initial

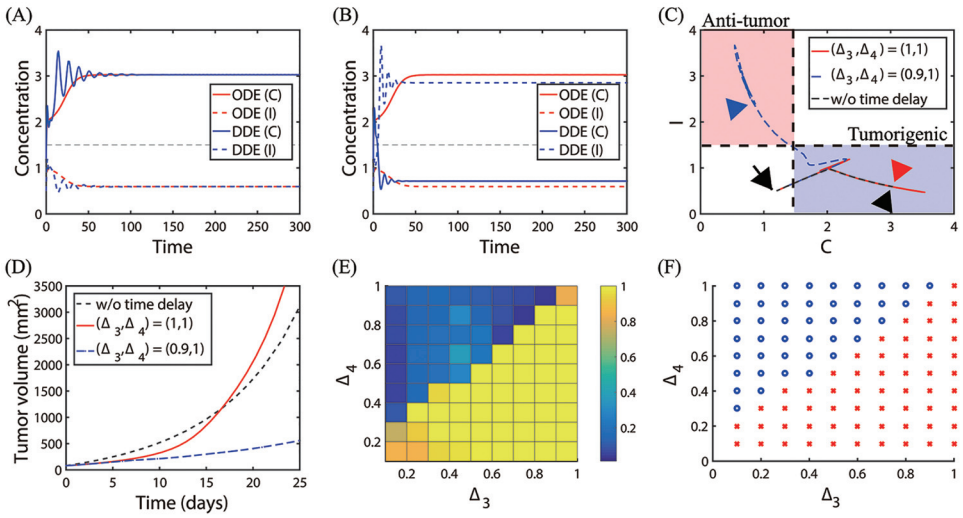

Fig 18. Dynamics of the system with time delays (Δ_3, Δ_4) in apoptosis of TANs. (A, B) Time courses of concentrations of two main variables (C, I) in the absence (ODE, red) and presence (DDE, blue) of time delays: $\Delta_3 = 1$, $\Delta_4 = 1$ in (A); $\Delta_3 = 0.9$, $\Delta_4 = 1.0$ in (B). (C) Trajectories of solutions ($C(t)$, $I(t)$) without (black dotted) and with ((Δ_3, Δ_4) = (1, 1) red solid; (Δ_3, Δ_4) = (0.9, 1) blue dashed) time delays in (A-B). (D) Time courses of the tumor volumes corresponding to (C). (E) Normalized tumor sizes for various strengths of the two time delays (Δ_3 and Δ_4). (F) Risk map of the time delay-induced transition of TANs from N2 to N1 phenotypes in the $\Delta_3 - \Delta_4$ plane. Blue circle = switching to the N1-dominant system. Red asterisk = persisting N2-dominant mode. Parameters: $S = 0.2$, $G = 0.4$. All other parameters are fixed as in Table 2. Initial condition: $T(0) = 0.2$, $C(0) = 1.2$, $I(0) = 0.5$.

https://doi.org/10.1371/journal.pone.0211041.g018

position was marked in black arrow. While the presence of time delays (Δ_3, Δ_4) = (1, 1) induces initial fluctuations (Fig 18A), the solutions converge to the N2-dominant steady states of ODEs (red arrowhead in Fig 18C). However, a slightly different combination of time delays ((Δ_3, Δ_4) = (0.9, 1)) leads to a phenotypic transition from the N2-dominant mode to the N1-dominant phase (blue arrowhead in Fig 18C) despite the initial fluctuation of solutions (blue curves in Fig 18B). Delayed apoptotic cell death leads to different tumor growth dynamics. Fig 18D shows time courses of the tumor volumes corresponding to three cases in Fig 18C. In the presence of time delays (Δ_3, Δ_4) = (1, 1), the tumor grows slower than the control (case without time delays) initially but the delay-induced oscillations push the TAN system to the N2-dominant phenotype faster than the control case around $t = 18$ *days*, leading to the larger N2-to-N1 ratio and faster tumor growth (red curve in Fig 18D). On the other hand, in the presence of time delays (Δ_3, Δ_4) = (0.9, 1), the tumor grows slower than the control due to strong suppression of the N2 module and enhancement of the N1 module. Fig 18E shows the normalized tumor size at $t = 25$ *days* for various strengths of the two time delays (Δ_3, $\Delta_4 \in$ [0, 1]) with a uniform length of 0.1. A *risk map* of time delay-induced transition of TANs from N2 to N1 phenotypes in the $\Delta_3 - \Delta_4$ plane is shown in Fig 18F. For a fixed value of Δ_3, an increase in Δ_4 results in the higher chance of transition to the $\mathbb{P}_a$-phase, thus slower tumor growth. On the other hand, for a fixed value of Δ_4, an increase in Δ_3 leads to a higher probability of transition to the $\mathbb{P}_t$-phase and faster tumor growth. To characterize the complex dynamics of the apoptotic cell death mechanism, we introduce the following Δ_4-to-Δ_3 ratio:

$$D_{ap} = \frac{\Delta_4}{\Delta_3} = \frac{\text{time delay in apoptosis of N1 TANs}}{\text{time delay in apoptosis of N2 TANs}}.$$

When D_{ap} is large, the delayed apoptotic process of N1 phenotypes and minimal delay in the apoptotic process of N2 phenotypes allow accumulation of more N1 TANs within the

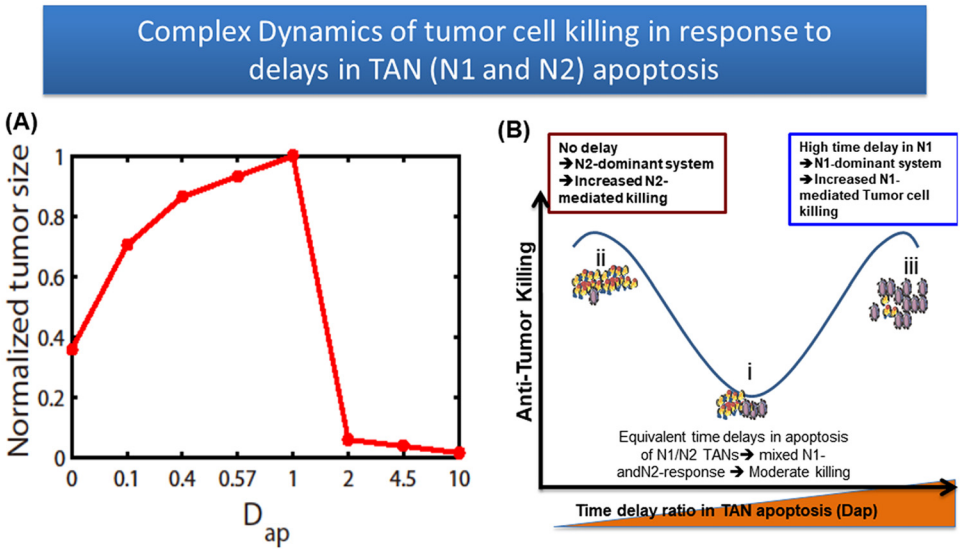

Fig 19. Effect of apoptosis delays of TANs in anti-tumor efficacy. (A) Tumor volume for various time delay ratios of TAN apoptosis (D_{ap}). (B) A model depicting the impact of D_{ap} on anti-tumor efficacy.

https://doi.org/10.1371/journal.pone.0211041.g019

microenvironment, pushing the system to the $\mathbb{P}_a$-phase and effective inhibition of tumor growth. On the other hand, a large delay in the apoptosis of N2 TANs with a relatively small delay in the apoptosis of N1 TANs, (*i.e.*, $D_{ap} \ll 1$), leads to significant accumulation of N2 TANs in the tumor microenvironment, leading to faster tumor growth.

Fig 19A shows the tumor volume for various D_{ap} at final time $t = 25\ day$. As D_{ap} is increased from the control value ($D_{ap} = 1$), the tumor size is significantly decreased. On the other hand, a decrease in D_{ap} also induces slower tumor growth, indicating the maximum tumor growth rate when $D_{ap} = 1$. The absence of the time delays in apoptosis signaling also induces slower tumor growth. Fig 19B illustrates a dynamic antitumor killing model with the relative time delay function D_{ap} as a key parameter. A relatively small delay ratio ($D_{ap} \ll 1$) (basic step i) induces phenotypic perturbations in N1- or N2-responses, which in turn decreases the N2-assisted tumor growth rate. On the other hand, the depletion of time delays in the apoptosis pathways of TANs (step ii) improved antitumor efficacy and suggests that the major antitumor response was likely due to the persistent N2-dominant microenvironment with quick clearance of TANs (Fig 18A). Our study also showed that complementing TANs with adjuvant N1 immunotherapy improved overall antitumor efficacy (step iii), through the facilitation of a robust N1-mediated tumor cell killing response beyond the limits of endogenous N2 TANs. In spite of a typical short half life of neutrophils, delayed apoptosis and accumulation of neutrophils in a tumor environment have been observed in other biological studies [93, 95, 96]. In particular, TANs often have a longer lifespan in the tumor microenvironment due to delayed apoptosis of TANs by modifying its signaling pathways involving FAS, ROS, active Caspase 3, 9, and Bcl-2 family [62]. Our mathematical model predicts that (i) D_{ap} can be used as a reliable diagnostic measure for aggressiveness of tumor progression; (ii) Anti-tumor efficacy can be improved by increasing the apoptosis decay of N1 TANs or by blocking the accumulation of N2 TANs in tumor microenvironment. In particular, drugs targeting apoptosis pathways of N1 TANs can effectively be used to enhance N1 neutrophil activities to reduce the tumor size.

Discussion

The immune system protects the host against various types of biological threats. However, it is well established that immune cells show functional plasticity in the context of cancer, and undergo phenotypic changes, promoting tumor growth and metastatic progression [74]. There have been substantial studies to pinpoint fundamental mechanisms through which TANs act on cancer progression [8, 17, 34], and especially via the coordination of chemotaxis-driven recruitment and activation of distinct immune cells to the tumor microenvironment [97–100] as well as immune suppression [74, 101, 102]. A groundbreaking work by Fridlender and colleagues [16] had illustrated that TGF-β in tumor microenvironment can generate a functional transition from the proinflammatory neutrophil phenotype (termed "N1") to the anti-inflammatory phenotype (termed "N2"); [74]. IL-6 also contributes to the formation of the N2 microenvironment [103, 104]. Neutrophil-to-lymphocyte ratio (NLR) was highly associated with progression in many cancer types [69] and has been suggested to be a prognostic factor (or biomarker) for various cancers including colorectal cancer [105, 106], nasopharyngeal carcinoma [107], non-small-cell lung cancer [71], breast cancer [108, 109], hepatocellular carcinoma [110], and melanoma [13]. Recently, it was shown that lung adenocarcinomas can promote bone stromal activity and increase bone mass even without bone metastasis, which in turn enhances tumor growth by remotely supplying tumor-infiltrating neutrophils [111]. However, how the systemic host environment can communicate with a tumor at a remote site is poorly understood.

Since TGF-β was identified as a master player that skews differentiation toward the N2 phenotype [16, 18, 19], TGF-β inhibitors are suggested to shift the TAN balance toward the N1 phenotype [20, 21]. In cancer research, type I IFNs (α and β) are substantially studied and tried for cancer therapy due to their anti-tumor capabilities by acting directly on cancer cells and through immunoregulatory characteristic [112]. These Type I IFNs can induce cell cycle arrest and apoptosis in several models [112–114] by acting on several signaling pathways including upregulation of p53 transcription [24]. Type I IFNs are suggested to mediate initial recruitment, active proliferation, phenotypic differentiation, and activation of various immune cells [115–118]. Interestingly, recent evidence from animal models has implicated that IFN-β signaling pathways play a critical role in inducing antitumor response in chemotherapy [119] and radiotherapy [68, 120]. Therefore, it is not surprising to see IFN-β gene transfer in extensive studies, due to the ability of IFN-β to improve (or normalize) immunological response in the tumor microenvironment [121–125]. IFN-mediated neutrophils was shown to upregulate PD-L1 and suppress T-cell proliferation [26].

We have developed a mathematical model by a system of ODEs and DDEs to study the effect of regulatory cytokines (TGF-β, IFN-β) and delayed apoptotic cell death mechanism on transitions between N1- and N2-dominant system, the N1/N2 mutual antagonism, and their impact on tumor growth (Fig 3). Mathematical analysis showed the complex, nonlinear behaviors of phenotypic switches between N1- and N2-dominant phases in response to fluctuating TGF-β and IFN-β, and tumor growth patterns (Figs 6–11). In particular, the bi-stability of the N1/N2 system generates a selection process of either promoting or suppressing tumor growth based on the initial distribution and phenotypic status of TANs in a tumor microenvironment (Figs 6 and 11). The microenvironmental pressure of inhibiting the phenotypes also determines the phenotypic switches (Figs 9–10). We also developed therapeutic strategies to control this complex network of TANs for slowing down tumor growth (Figs 13–16). Even though high-dose IFNs were suggested to the only available therapy for relapse-free benefits and overall survival (OS) [126], the administration of high-dose IFN in cancer patients in stage IIb/III needs to be considered carefully [112]. High-dose IFN is not always considered as the first line

of treatment option for melanoma patients due to a lack of substantial evidence supporting a long-term OS merit and the extensive associated toxicity [83–86]. Therefore, it is necessary to establish optimal dose and treatment duration of IFNs despite extensive clinical experience [112]. In this study, we investigated the optimal dose schedule of IFN-β in the absence or presence of an alternative drug, the TGF-β inhibitor (Fig 15). In our mathematical framework, the high N2-to-N1 ratio (equivalent to NLR) was highly associated with faster tumor growth and worse clinical outcomes (Fig 15). Experimental studies [22–25, 36, 38] are in good agreement with the conclusions of the mathematical model. The optimal strategies of reducing the tumor size with minimal side effects [78, 85–89] and maximal antitumor efficacy were explored by using the TGF-β inhibitor only, IFN-β only, and the combination (TGF-β inhibitor + IFN-β) therapy (Fig 16).

The life span of neutrophils is strictly regulated in order to maintain tissue homeostasis due to their potential toxicity [127]. These cells are quickly removed from circulation after leaving the bone marrow with a very short half life. However, several proinflammatory cytokines were reported to influence their longevity [128, 129]. There are also many cellular and molecular factors that may affect delays in signaling pathways, apoptosis, and inhibition of neutrophils in the given microenvironment [93–95]. For example, external (smoking and nicotine) and internal (ROS) factors were shown to delay neutrophil apoptosis by suppressing signaling pathways (InsP7, Akt, ROS) in lung diseases such as COPD and lung cancers [93, 95, 96]. Recently, it was also shown that ROS production is reduced in the absence of endogenous IFN-β, causing the delayed apoptosis of TANs [62]. Interestingly, a recent study showed that a radiation therapy (RT) can induce the polarization of N1 TANs and reactive oxygen species induced by RT damage tumor tissues, which overall improves anti-tumor efficacy [130]. These microenvironmental factors delay the inhibition and apoptosis of both types of TANs, inducing a complex imbalance between N1 and N2 phenotypes. The mathematical model predicted that various combinations of two time delays in inhibition of signaling pathways within those TANs will induce the relative imbalance between N1 and N2-dominant phases, leading to promotion or suppression of aggressive tumor growth (Fig 17).

We have shown that typical therapy can be exploited by manipulating the delay of apoptosis pathways of both types of TANs. By reducing the relative ratio of apoptosis delay of N1 and N2 TANs, or by increasing time delay of apoptotic pathways of N1 TANs, the efficacy of the anti-tumor treatment is increased. The mathematical model also predicts that the absence of time delays in apoptosis may allow a greater chance to induce N1 TANs in response to intermediate levels of TGF-β, thereby increasing antitumor efficacy (Fig 18). In particular, the model predicted that either strategy, i.e., induction of small (or none) delay of N2 TANs or large delay of N1 TANs, increased the survival rate (Fig 19), even though it is not clear which of the two strategies is clinically better. The answer should also depend on negative side effects associated with the delays of TANs (mixed N1/N2 immune response) and with the injection of apoptosis-targeting drugs (toxicity and inflammation). Our results provide a scientific basis for targeting suppressive effect of N2 TANs by normalizing immune activities (increase in α or decrease in β) within the tumor microenvironment or keeping a favorable balance of the N1/N2 TAN's properties toward N1 TANs [35]. While blood normalization was suggested to be an alternative concept of creating an anti-tumor microenvironment including N1 TANs [75, 76], more innovative platforms of normalizing the immune system need to be invented.

In this work, we did not specifically consider many other microenvironmental players such as signaling networks [131], human neutrophil elastase as a therapeutic target in the absence [132, 133] and presence [134] of LPS, endogenous NK immune dynamics [40, 135], angiogenesis from blood vessels [136–138], ECM remodeling [139], or growth factors such as epidermal growth factor (EGF) [140, 141], and CSF-1 [7, 142]. These factors may play critical roles in

cancer progression. For example, neutrophil elastin (NE) was shown to indirectly promote the tumor growth by stimulating the PI3K signaling pathways in lung cancer cells [143]. Neutrophil extracellular traps (NETs) were abundant in tumour sections and induce the transformation of B cells [144], contributing to cancer progression [145]. However, another study [146] suggested that the NETs suppressed tumor growth in colonic adenocarcinoma. It is possible that unforeseen microenvironmental factors could have an effect on our approach (governing equations and the many estimated values for mathematical and biological variables). For example, in our model, it is assumed that the tumor microenvironment neutrophils can switch freely from N1 to N2 TANs or from N2 to N1 TANs, given a specific biochemical stimulus. However in vivo there may be unknown biochemical limits to these transitions, such as factors that stabilize one state or another after it has been established. This could be the presence of NETs and associated pro-inflammatory factors. The exact role of this biochemical structural device in regulation of promotion [147–150] or suppression of tumor progression [146] still remains controversial. Our model, however, provides a starting point of the general framework of those key transitions between N1 and N2 TANs in response to known key players. We also plan to investigate the role of the possibly continuous spectrum of the N1 → N2 transition. Further investigation and experimental validation need to be done as more experimental data are available. A multi-scale mathematical model [64, 151–156] could be used to take into account inter and intra-cellular signaling regulation at the microscale level and integrating those to stromal cells and tumor cells at the cellular level. However, the mathematical model in this paper is a first step toward further understanding of lung cancer development in a tumor microenvironment and further experimental investigation. We hope to address these issues in future work.

Supporting information

S1 Appendix. Analysis of the model: Effect of N1 immunity on cancer cell killing.
(PDF)

Acknowledgments

This paper was supported by Konkuk University in 2015 (Yangjin Kim).

Author Contributions

Conceptualization: Yangjin Kim.

Formal analysis: Donggu Lee, Seongwon Lee.

Investigation: Yangjin Kim, Donggu Lee.

Software: Junho Lee.

Visualization: Junho Lee.

Writing – original draft: Yangjin Kim.

Writing – review & editing: Yangjin Kim, Sean Lawler.

References

1. Torre LA, Bray F, Siegel RL, Ferlay J, Lortet-Tieulent J, Jemal A. Global cancer statistics. CA Cancer J Clin. 2015; 65(2):87–108. https://doi.org/10.3322/caac.21262 PMID: 25651787

2. Molina JR, Yang P, Cassivi SD, Schild SE, Adjei AA. Non-small cell lung cancer: epidemiology, risk factors, treatment, and survivorship. Mayo Clin Proc. 2008; 83(5):584–594. https://doi.org/10.4065/83.5.584 PMID: 18452692
3. Mantovani A, Sozzani S, Locati M, Allavena P, Sica A. Macrophage polarization: tumor-associated macrophages as a paradigm for polarized M2 mononuclear phagocytes. Trends Immunol. 2002; 23(11):549–55. https://doi.org/10.1016/S1471-4906(02)02302-5 PMID: 12401408
4. Balkwill F, Coussens LM. Cancer: an inflammatory link. Nature. 2004; 431(7007):405–6. https://doi.org/10.1038/431405a PMID: 15385993
5. Luo Y, Zhou H, Krueger J, Kaplan C, Lee SH, Dolman C, et al. Targeting tumor-associated macrophages as a novel strategy against breast cancer. J Clin Invest. 2006; 116(8):2132–2141. https://doi.org/10.1172/JCI27648 PMID: 16862213
6. Yuan A, Hsiao YJ, Chen HY, Chen HW, Ho CC, Chen YY, et al. Opposite Effects of M1 and M2 Macrophage Subtypes on Lung Cancer Progression. Sci Rep. 2015; 5:14273. https://doi.org/10.1038/srep14273 PMID: 26399191
7. Kim Y, Jeon H, Othmer HG. The role of the tumor microenvironment in glioblastoma: A mathematical model. IEEE Trans Biomed Eng. 2017; 64(3):519–527. https://doi.org/10.1109/TBME.2016.2637828 PMID: 27959794
8. Shaul ME, Levy L, Sun J, Mishalian I, Singhal S, Kapoor V, et al. Tumor-associated neutrophils display a distinct N1 profile following TGFbeta modulation: A transcriptomics analysis of pro- vs. antitumor TANs. Oncoimmunology. 2016; 5(11). https://doi.org/10.1080/2162402X.2016.1232221 PMID: 27999744
9. Hagerling C, Werb Z. Neutrophils: Critical components in experimental animal models of cancer. Semin Immunol. 2016; 28(2):197–204. https://doi.org/10.1016/j.smim.2016.02.003 PMID: 26976824
10. Sionov RV, Fridlender ZG, Granot Z. The multifaceted roles neutrophils play in the tumor microenvironment. Cancer Microenviron. 2015; 3:125–158. https://doi.org/10.1007/s12307-014-0147-5
11. Swierczak A, Mouchemore KA, Hamilton JA, Anderson RL. Neutrophils: important contributors to tumor progression and metastasis. Cancer Metast Rev. 2015; 34:735–751. https://doi.org/10.1007/s10555-015-9594-9
12. Liang W, Ferrara N. The complex role of neutrophils in tumor angiogenesis and metastasis. Cancer Immunol Res. 2016; 4:83–91. https://doi.org/10.1158/2326-6066.CIR-15-0313 PMID: 26839309
13. Schmidt H, Bastholt L, Geertsen P, Christensen IJ, Larsen S, Gehl J, et al. Elevated neutrophil and monocyte counts in peripheral blood are associated with poor survival in patients with metastatic melanoma: a prognostic model. Br J Cancer. 2005; 93(3):273–8. https://doi.org/10.1038/sj.bjc.6602702 PMID: 16052222
14. Bellocq A, Antoine M, Flahault A, Philippe C, Crestani B, Bernaudin JF, et al. Neutrophil alveolitis in bronchioloalveolar carcinoma: induction by tumor-derived interleukin-8 and relation to clinical outcome. Am J Pathol. 1998; 152(1):83–92. PMID: 9422526
15. Atzpodien J, Reitz M. Peripheral blood neutrophils as independent immunologic predictor of response and long-term survival upon immunotherapy in metastatic renal-cell carcinom. Cancer Biother Radiopharm. 2008; 23(1):129–34. https://doi.org/10.1089/cbr.2007.0429 PMID: 18298337
16. Fridlender ZG, Sun J, Kim S, Kapoor V, Cheng G, Ling L, et al. Polarization of tumor-associated neutrophil phenotype by TGF-beta: N1 versus N2 TAN. Cancer Cell. 2009; 16(3):183–194. https://doi.org/10.1016/j.ccr.2009.06.017 PMID: 19732719
17. Tuting T, de Visser KE. CANCER. How neutrophils promote metastasis. Science. 2016; 352(6282):145–146. https://doi.org/10.1126/science.aaf7300 PMID: 27124439
18. Saha S, Biswas SK. Tumor-Associated Neutrophils Show Phenotypic and Functional Divergence in Human Lung Cancer. Cancer Cell. 2016; 30(1):11–13. https://doi.org/10.1016/j.ccell.2016.06.016 PMID: 27411583
19. Shen L, Smith JM, Shen Z, Eriksson M, Sentman C, Wira CR. Inhibition of human neutrophil degranulation by transforming growth factor-beta1. Clin Exp Immunol. 2007; 149:155–161. https://doi.org/10.1111/j.1365-2249.2007.03376.x PMID: 17403059
20. Andzinski L, Kasnitz N, Stahnke S, Wu CF, Gereke M, von Kockritz-Blickwede M, et al. Type I IFNs induce anti-tumor polarization of tumor associated neutrophils in mice and human. Int J Cancer. 2016; 138:1982–93. https://doi.org/10.1002/ijc.29945 PMID: 26619320
21. Jablonska J, Leschner S, Westphal K, Lienenklaus S, Weiss S. Neutrophils responsive to endogenous IFN-beta regulate tumor angiogenesis and growth in a mouse tumor model. J Clin Invest. 2010; 120(4):1151–64. https://doi.org/10.1172/JCI37223 PMID: 20237412
22. Studeny M, Marini FC, Dembinski JL, Zompetta C, Cabreira-Hansen M, Bekele BN, et al. Mesenchymal stem cells: potential precursors for tumor stroma and targeted-delivery vehicles for anticancer

agents. J Natl Cancer Inst. 2004; 96(21):1593–603. https://doi.org/10.1093/jnci/djh299 PMID: 15523088

23. Chiantore MV, Vannucchi S, Accardi R, Tommasino M, Percario ZA, Vaccari G, et al. Interferon-β induces cellular senescence in cutaneous human papilloma virus-transformed human keratinocytes by affecting p53 transactivating activity. PLoS One. 2012; 7(5):e36909. https://doi.org/10.1371/journal.pone.0036909 PMID: 22615843

24. Takaoka A, Hayakawa S, Yanai H, Stoiber D, Negishi H, Kikuchi H, et al. Integration of interferon-alpha/beta signalling to p53 responses in tumour suppression and antiviral defence. Nature. 2003; 424(6948):516–23. https://doi.org/10.1038/nature01850 PMID: 12872134

25. Zhang F, Sriram S. Identification and characterization of the interferon-beta-mediated p53 signal pathway in human peripheral blood mononuclear cells. Immunology. 2009; 128(1 Suppl):e905–18. https://doi.org/10.1111/j.1365-2567.2009.03104.x PMID: 19740351

26. de Kleijn S, Langereis JD, Leentjens J, Kox M, Netea MG, Koenderman L, et al. IFN-γ-stimulated neutrophils suppress lymphocyte proliferation through expression of PD-L1. PLoS One. 2013; 8(8): e72249. https://doi.org/10.1371/journal.pone.0072249 PMID: 24015224

27. Garcia-Diaz A, Shin DS, Moreno BH, Saco J, Escuin-Ordinas H, Rodriguez GA, et al. Interferon Receptor Signaling Pathways Regulating PD-L1 and PD-L2 Expression. Cell Rep. 2017; 19(6):1189–1201. https://doi.org/10.1016/j.celrep.2017.04.031 PMID: 28494868

28. Patel MR, Jacobson BA, Ji Y, Drees J, Tang S, Xiong K, et al. Vesicular stomatitis virus expressing interferon-β is oncolytic and promotes antitumor immune responses in a syngeneic murine model of non-small cell lung cancer. Oncotarget. 2015; 6(32):33165–77. https://doi.org/10.18632/oncotarget.5320 PMID: 26431376

29. Horie M, Saito A, Mikami Y, Ohshima M, Morishita Y, Nakajima J, et al. Characterization of human lung cancer-associated fibroblasts in three-dimensional in vitro co-culture model. Biochem Biophys Res Commun. 2012; 423(1):158–63. https://doi.org/10.1016/j.bbrc.2012.05.104 PMID: 22634307

30. Liao D, Luo Y, Markowitz D, Xiang R, Reisfeld RA. Cancer associated fibroblasts promote tumor growth and metastasis by modulating the tumor immune microenvironment in a 4T1 murine breast cancer model. PLoS One. 2009; 4(11):e7965. https://doi.org/10.1371/journal.pone.0007965 PMID: 19956757

31. Madar S, Harel E, Goldstein I, Stein Y, Kogan-Sakin I, Kamer I, et al. Mutant p53 attenuates the anti-tumorigenic activity of fibroblasts-secreted interferon beta. PLoS One. 2013; 8(4):e61353. https://doi.org/10.1371/journal.pone.0061353 PMID: 23630584

32. Pelletier M, Maggi L, Micheletti A, Lazzeri E, Tamassia N, Costantini C, et al. Evidence for a cross-talk between human neutrophils and Th17 cells. Blood. 2010; 115(2):335–43. https://doi.org/10.1182/blood-2009-04-216085 PMID: 19890092

33. Mantovani A, Cassatella MA, Costantini C, Jaillon S. Neutrophils in the activation and regulation of innate and adaptive immunity. Nat Rev Immunol. 2011; 11(8):519–31. https://doi.org/10.1038/nri3024 PMID: 21785456

34. Powell DR, Huttenlocher A. Neutrophils in the Tumor Microenvironment. Trends Immunol. 2016; 37(1):41–52. https://doi.org/10.1016/j.it.2015.11.008 PMID: 26700397

35. Shaul ME, Fridlender ZG. Cancer related circulating and tumor-associated neutrophils - subtypes, sources and function. FEBS J. 2018;Epub ahead of print. https://doi.org/10.1111/febs.14524 PMID: 29851227

36. Catani JPP, Medrano RFV, Hunger A, Valle PD, Adjemian S, Zanatta DB, et al. Intratumoral Immunization by p19Arf and Interferon-beta Gene Transfer in a Heterotopic Mouse Model of Lung Carcinoma. Transl Oncol. 2016; 9(6):565–574. https://doi.org/10.1016/j.tranon.2016.09.011 PMID: 27916291

37. Ghosh D, Parida P. Interferon Therapy in Lung Cancer: Current Perspectives. Current Cancer Therapy Reviews. 2016; 12(4):237–245. https://doi.org/10.2174/1573394713666170316124158

38. Serizawa M, Takahashi T, Yamamoto N, Koh Y. Combined treatment with erlotinib and a transforming growth factor-β type I receptor inhibitor effectively suppresses the enhanced motility of erlotinib-resistant non-small-cell lung cancer cells. J Thorac oncol. 2013; 8(3):259–69. https://doi.org/10.1097/JTO.0b013e318279e942 PMID: 23334091

39. Demidenko E. Mixed Models: Theory and Applications with R. 2nd ed. Wiley Series; 2013.

40. Kim Y, Yoo JY, Lee TJ, Liu J, Yu J, Caligiuri MA, et al. Complex role of NK cells in regulation of oncolytic virus-bortezomib therapy. Proc Natl Acad Sci USA. 2018; 115(19):4927–4932. https://doi.org/10.1073/pnas.1715295115 PMID: 29686060

41. Kim Y, Wallace J, Li F, Ostrowski M, Friedman A. Transformed epithelial cells and fibroblasts/myofibroblasts interaction in breast tumor: a mathematical model and experiments. J Math Biol. 2010; 61(3):401–421. https://doi.org/10.1007/s00285-009-0307-2 PMID: 19902212

42. Stein AM, Demuth T, Mobley D, Berens M, Sander LM. A mathematical model of glioblastoma tumor spheroid invasion in a three-dimensional in vitro experiment. Biophys J. 2007; 92(1):356–65. https://doi.org/10.1529/biophysj.106.093468 PMID: 17040992

43. Enderling H, Anderson AR, Chaplain MA, Munro AJ, Vaidya JS. Mathematical modelling of radiotherapy strategies for early breast cancer. J Theor Biol. 2006; 241(1):158–71. https://doi.org/10.1016/j.jtbi.2005.11.015 PMID: 16386275

44. Weis JA, Miga MI, Yankeelov TE. Three-dimensional Image-based Mechanical Modeling for Predicting the Response of Breast Cancer to Neoadjuvant Therapy. Comput Methods Appl Mech Eng. 2017; 314:494–512. https://doi.org/10.1016/j.cma.2016.08.024 PMID: 28042181

45. Enderling H, Chaplain MA, Anderson AR, Vaidya JS. A mathematical model of breast cancer development, local treatment and recurrence. J Theor Biol. 2007; 246(2):245–59. https://doi.org/10.1016/j.jtbi.2006.12.010 PMID: 17289081

46. Corwin D, Holdsworth C, Rockne RC, Trister AD, Mrugala MM, Rockhill JK, et al. Toward patient-specific, biologically optimized radiation therapy plans for the treatment of glioblastoma. PLoS One. 2013; 8(11). https://doi.org/10.1371/journal.pone.0079115 PMID: 24265748

47. Kim Y, Friedman A. Interaction of tumor with its microenvironment: A Mathematical Model. Bull Math Biol. 2010; 72(5):1029–1068. https://doi.org/10.1007/s11538-009-9481-z PMID: 19908100

48. Maini P. Modelling Aspects of Tumour Metabolism. Proc Int Cong Mathematicians. 2010;Indiana.

49. Kim Y, Lee HG, Dmitrieva N, Kim J, Kaur B, Friedman A. Choindroitinase ABC I-mediated enhancement of oncolytic virus spread and anti-tumor efficacy: A mathematical model. PLoS One. 2014; 9(7): e102499. https://doi.org/10.1371/journal.pone.0102499 PMID: 25047810

50. Swanson KR, Alvord EC, Murray JD. Virtual resection of gliomas: Effect of extent of resection on recurrence. Math Comp Modelling. 2003; 37:1177–1190. https://doi.org/10.1016/S0895-7177(03)00129-8

51. Kim Y, Roh S, Lawler S, Friedman A. miR451 and AMPK/MARK mutual antagonism in glioma cells migration and proliferation. PLoS One. 2011; 6(12):e28293.

52. von Vietinghoff S, Ley K. Homeostatic regulation of blood neutrophil counts. J Immunol. 2008; 181(8):5183–8. https://doi.org/10.4049/jimmunol.181.8.5183 PMID: 18832668

53. Price TH, Dale DC. Neutrophil preservation: the effect of short-term storage on in vivo kinetics. J Clin Invest. 1977; 59(3):475–80. https://doi.org/10.1172/JCI108662 PMID: 838860

54. Rosenshein MS, Price TH DD. Neutropenia, inflammation, and the kinetics of transfused neutrophils in rabbits. J Clin Invest. 1979; 64:580–585. https://doi.org/10.1172/JCI109496 PMID: 457870

55. Basu S, Hodgson G, Katz M, Dunn AR. Evaluation of role of G-CSF in the production, survival, and release of neutrophils from bone marrow into circulation. Blood. 2002; 100:854–861. https://doi.org/10.1182/blood.V100.3.854 PMID: 12130495

56. Price TH, Chatta GS, Dale DC. Effect of recombinant granulocyte colony-stimulating factor on neutrophil kinetics in normal young and elderly humans. Blood. 1996; 88:335–340. PMID: 8704192

57. Cartwright GE, Athens JW, Wintrobe MM. The Kinetics Of Granulopoiesis In Normal Man. Blood. 1964; 24:780–803. PMID: 14235362

58. Tak T, Tesselaar K, Pillay J, Borghans JA, Koenderman L. What's your age again? Determination of human neutrophil half-lives revisited. J Leukoc Biol. 2013; 94(4):595–601. https://doi.org/10.1189/jlb.1112571 PMID: 23625199

59. Pillay J, den Braber I, Vrisekoop N, Kwast LM, de Boer RJ, Borghans JA, et al. In vivo labeling with $^{2}H_{2}O$ reveals a human neutrophil lifespan of 5.4 days. Blood. 2010; 116:625–627. https://doi.org/10.1182/blood-2010-01-259028 PMID: 20410504

60. Dale DC, Liles WC, Llewellyn C, Rodger E, Price TH. Neutrophil transfusions: kinetics and functions of neutrophils mobilized with granulocyte-colony-stimulating factor and dexamethasone. Transfusion. 1998; 38:713–721. https://doi.org/10.1046/j.1537-2995.1998.38898375509.x PMID: 9709778

61. Steinbach KH, Schick P, Trepel F, Raffler H, Dohrmann J, Heilgeist G, et al. Estimation of kinetic parameters of neutrophilic, eosinophilic, and basophilic granulocytes in human blood. Blut. 1979; 39:27–38. https://doi.org/10.1007/BF01008072 PMID: 223692

62. Andzinski L, Wu CF, Lienenklaus S, Kroger A, Weiss S, Jablonska J. Delayed apoptosis of tumor associated neutrophils in the absence of endogenous IFN-β. International Journal of Cancer. 2015; 136(3):572–583. https://doi.org/10.1002/ijc.28957 PMID: 24806531

63. Granot Z, Jablonska J. Distinct Functions of Neutrophil in Cancer and Its Regulation. Mediators Inflamm. 2015; 2015(701067):1–11. https://doi.org/10.1155/2015/701067

64. Kim Y, Othmer HG. A hybrid model of tumor-stromal interactions in breast cancer. Bull Math Biol. 2013; 75:1304–1350. https://doi.org/10.1007/s11538-012-9787-0 PMID: 23292359

65. Herbertz S, Sawyer JS, Stauber AJ, Gueorguieva I, Driscoll KE, Estrem ST, et al. Clinical development of galunisertib (LY2157299 monohydrate), a small molecule inhibitor of transforming growth factor-beta signaling pathway. Drug Design, Development and Therapy. 2015; 9:4479–4499. https://doi.org/10.2147/DDDT.S86621 PMID: 26309397

66. McKenna SD, Vergilis K, Arulanandam AR, Weiser WY, Nabioullin R, Tepper MA. Formation of human IFN-beta complex with the soluble type I interferon receptor IFNAR-2 leads to enhanced IFN stability, pharmacokinetics, and antitumor activity in xenografted SCID mice. J Interferon Cytokine Res. 2004; 24(2):119–29. https://doi.org/10.1089/107999004322813363 PMID: 14980076

67. Salmon P, Cotonnec JYL, Galazka A, Abdul-Ahad A, Darragh A. Pharmacokinetics and pharmacodynamics of recombinant human interferon-beta in healthy male volunteers. J Interferon Cytokine Res. 1996; 16(10):759–64. https://doi.org/10.1089/jir.1996.16.759 PMID: 8910759

68. Deng L, Liang H, Xu M, Yang X, Burnette B, Arina A, et al. STING-Dependent Cytosolic DNA Sensing Promotes Radiation-Induced Type I Interferon-Dependent Antitumor Immunity in Immunogenic Tumors. Immunity. 2014; 41(5):843–52. https://doi.org/10.1016/j.immuni.2014.10.019 PMID: 25517616

69. Chen Y, Yan H, Wang Y, Shi Y, Dai G. Significance of baseline and change in neutrophil-to-lymphocyte ratio in predicting prognosis: a retrospective analysis in advanced pancreatic ductal adenocarcinoma. Sci Rep. 2017; 7(1):753. https://doi.org/10.1038/s41598-017-00859-5 PMID: 28392554

70. Zeren S, Yaylak F, Ozbay I, Bayhan Z. Relationship Between the Neutrophil to Lymphocyte Ratio and Parathyroid Adenoma Size in Patients With Primary Hyperparathyroidism. Int Surg. 2015; 100(7–8):1185–9 PMID: 26595491

71. Peng B, Wang YH, Liu YM, Ma LX. Prognostic significance of the neutrophil to lymphocyte ratio in patients with non-small cell lung cancer: a systemic review and meta-analysis. Int J Clin Exp Med. 2015; 8(3):3098–106. PMID: 26064198

72. Shimizu K, Okita R, Saisho S, Maeda A, Nojima Y, Nakata M. Preoperative neutrophil/lymphocyte ratio and prognostic nutritional index predict survival in patients with non-small cell lung cancer. World J Surg Oncol. 2015; 13:291. https://doi.org/10.1186/s12957-015-0710-7 PMID: 26424708

73. Huang QT, Man QQ, Hu J, Yang YL, Zhang YM, Wang W, et al. Prognostic significance of neutrophil-to-lymphocyte ratio in cervical cancer: A systematic review and meta-analysis of observational studies. Oncotarget. 2017; 8(10):16755–16764. https://doi.org/10.18632/oncotarget.15157 PMID: 28187430

74. Granot Z, Fridlender ZG. Plasticity beyond cancer cells and the immunosuppressive switch. Cancer Res. 2015; 75(21):4441–5. https://doi.org/10.1158/0008-5472.CAN-15-1502 PMID: 26475869

75. Gordon-Weeks AN, Lim SY, Yuzhalin AE, Jones K, Markelc B, Kim KJ, et al. Neutrophils promote hepatic metastasis growth through fibroblast growth factor 2-dependent angiogenesis in mice. Hepatology. 2017; 65(6):1920–1935. https://doi.org/10.1002/hep.29088 PMID: 28133764

76. Schaaf MB, Garg AD, Agostinis P. Defining the role of the tumor vasculature in antitumor immunity and immunotherapy. Cell Death Dis. 2018; 9(2):115. https://doi.org/10.1038/s41419-017-0061-0 PMID: 29371595

77. Marino S, Hogue IB, Ray CJ, Kirschner DE. A methodology for performing global uncertainty and sensitivity analysis in systems biology. Journal of Theoretical Biology. 2008; 254(1):178–196. https://doi.org/10.1016/j.jtbi.2008.04.011 PMID: 18572196

78. Jonasch E, Haluska FG. Interferon in oncological practice: review of interferon biology, clinical applications, and toxicities. Oncologist. 2001; 6(1):34–55. https://doi.org/10.1634/theoncologist.6-1-34 PMID: 11161227

79. Tavakoli M, Manshadi SMP, Naderi N, Dehghan A, Azizi S. Unusual side effects of interferon Beta-1a in patient with multiple sclerosis. Mater Sociomed. 2012; 24(3):203–5. https://doi.org/10.5455/msm.2012.24.203-205 PMID: 23922529

80. Essers MA, Offner S, Blanco-Bose WE, Waibler Z, Kalinke U, Duchosal MA, et al. IFNalpha activates dormant haematopoietic stem cells in vivo. Nature. 2009; 458(7240):904–908. https://doi.org/10.1038/nature07815 PMID: 19212321

81. Parker BS, Rautela J, Hertzog PJ. Antitumour actions of interferons: implications for cancer therapy. Nat Rev Cancer. 2016; 16(3):131–144. https://doi.org/10.1038/nrc.2016.14 PMID: 26911188

82. Brockwell NK, Owen KL, Zanker D, Spurling A, Rautela J, Duivenvoorden HM, et al. Neoadjuvant Interferons: Critical for Effective PD-1-Based Immunotherapy in TNBC. Cancer Immunol Res. 2017; 5(10):871–884. https://doi.org/10.1158/2326-6066.CIR-17-0150 PMID: 28848054

83. Lens MB, Dawes M. Interferon alfa therapy for malignant melanoma: a systematic review of randomized controlled trials. J Clin Oncol. 2002; 20(7):1818–25. https://doi.org/10.1200/JCO.2002.07.070 PMID: 11919239

84. Wheatley K, Ives N, Hancock B, Gore M, Eggermont A, Suciu S. Does adjuvant interferon-alpha for high-risk melanoma provide a worthwhile benefit? A meta-analysis of the randomised trials. Cancer Treat Rev. 2003; 29(4):241–252. https://doi.org/10.1016/S0305-7372(03)00074-4 PMID: 12927565

85. Kirkwood JM, Manola J, Ibrahim J, Sondak V, Ernstoff MS, Rao U. A pooled analysis of eastern cooperative oncology group and intergroup trials of adjuvant high-dose interferon for melanoma. Clin Cancer Res. 2004; 10(5):1670–1677. https://doi.org/10.1158/1078-0432.CCR-1103-3 PMID: 15014018

86. Bajetta E. Adjuvant use of interferon alpha 2b is not justified in patients with stage IIb/III melanoma. Nat Clin Pract Oncol. 2008; 5(1):4–5. https://doi.org/10.1038/ncponc1007 PMID: 18043604

87. Kingwell E, Evans C, Zhu F, Oger J, Hashimoto S, Tremlett H. Assessment of cancer risk with beta-interferon treatment for multiple sclerosis. J Neurol Neurosurg Psychiatry. 2014; 85(10):1096–1102. https://doi.org/10.1136/jnnp-2013-307238 PMID: 24594506

88. Connolly EC, Freimuth J, Akhurst RJ. Complexities of TGF-β targeted cancer therapy. International journal of biological sciences. 2012; 8(7):964. https://doi.org/10.7150/ijbs.4564 PMID: 22811618

89. Calone I, Souchelnytskyi S. Inhibition of TGFbeta signaling and its implications in anticancer treatments. Exp Oncol. 2012; 34(1):9–16. PMID: 22453142

90. Doherty MR, Jackson MW. The Critical, Clinical Role of Interferon-Beta in Regulating Cancer Stem Cell Properties in Triple-Negative Breast Cancer. DNA Cell Biol. 2018; 37(6):513–516. https://doi.org/10.1089/dna.2018.4247 PMID: 29750542

91. Ohshio Y, Teramoto K, Hashimoto M, Kitamura S, Hanaoka J, Kontani K. Inhibition of transforming growth factor-beta release from tumor cells reduces their motility associated with epithelial-mesenchymal transition. Oncol Rep. 2013; 30(2):1000–1006. https://doi.org/10.3892/or.2013.2505 PMID: 23715805

92. Okada Y, Wang T, Kasai K, Suzuki K, Takikawa Y. Regulation of transforming growth factor is involved in the efficacy of combined 5-fluorouracil and interferon alpha-2b therapy of advanced hepatocellular carcinoma. Cell Death Discov. 2018; 4::42. https://doi.org/10.1038/s41420-018-0040-y PMID: 29560281

93. Xu Y, Li H, Bajrami B, Kwak H, Cao S, Liu P, et al. Cigarette smoke (CS) and nicotine delay neutrophil spontaneous death via suppressing production of diphosphoinositol pentakisphosphate. Proc Natl Acad Sci USA. 2013; 110(19):7726–7731. https://doi.org/10.1073/pnas.1302906110 PMID: 23610437

94. Kuijpers T, Lutter R. Inflammation and repeated infections in CGD: two sides of a coin. Cell Mol Life Sci. 2012; 69(1):7–15. https://doi.org/10.1007/s00018-011-0834-z PMID: 22083605

95. Kasahara Y, Iwai K, Yachie A, Ohta K, Konno A, Seki H, et al. Involvement of reactive oxygen intermediates in spontaneous and CD95 (Fas/APO-1)-mediated apoptosis of neutrophils. Blood. 1997; 89(5):1748–1753. PMID: 9057659

96. Dibbert B, Weber M, Nikolaizik WH, Vogt P, Schoni MH, Blaser K, et al. Cytokine-mediated Bax deficiency and consequent delayed neutrophil apoptosis: a general mechanism to accumulate effector cells in inflammation. Proc Natl Acad Sci USA. 1999; 96(23):13330–13335. https://doi.org/10.1073/pnas.96.23.13330 PMID: 10557320

97. Scapini P, Lapinet-Vera JA, Gasperini S, Calzetti F, Bazzoni F, Cassatella MA. The neutrophil as a cellular source of chemokines. Immunol Rev. 2000; 177:195–203. https://doi.org/10.1034/j.1600-065X.2000.17706.x PMID: 11138776

98. Gabrilovich D, Nagaraj S. Myeloid-derived suppressor cells as regulators of the immune system. Nat Rev Immunol. 2009; 9(3):162–174. https://doi.org/10.1038/nri2506 PMID: 19197294

99. Gregory AD, Houghton AM. Tumor-associated neutrophils: new targets for cancer therapy. Cancer Res. 2011; 71(7):2411–6. https://doi.org/10.1158/0008-5472.CAN-10-2583 PMID: 21427354

100. Tecchio C, Micheletti A, Cassatella MA. Neutrophil-derived cytokines: facts beyond expression. Front Immunol. 2014; 5:508. https://doi.org/10.3389/fimmu.2014.00508 PMID: 25374568

101. Sagiv JY, Michaeli J, Assi S, Mishalian I, Kisos H, Levy L, et al. Phenotypic diversity and plasticity in circulating neutrophil subpopulations in cancer. Cell Rep. 2015; 10(4):562–73. https://doi.org/10.1016/j.celrep.2014.12.039 PMID: 25620698

102. Coffelt SB, Kersten K, Doornebal CW, Weiden J, Vrijland K, Hau CS, et al. IL-17-producing $\gamma\delta$ T cells and neutrophils conspire to promote breast cancer metastasis. Nature. 2015; 522(7556):345–348. https://doi.org/10.1038/nature14282 PMID: 25822788

103. Yan B, Wei JJ, Yuan Y, Sun R, Li D, Luo J, et al. IL-6 cooperates with G-CSF to induce protumor function of neutrophils in bone marrow by enhancing STAT3 activation. J Immunol. 2013; 190(11):5882–5893. https://doi.org/10.4049/jimmunol.1201881 PMID: 23630344

104. Zhou L, Ivanov II, Spolski R, Min R, Shenderov K, Egawa T, et al. IL-6 programs T_H-17 cell differentiation by promoting sequential engagement of the IL-21 and IL-23 pathways. Nat Immunol. 2007; 8 (9):967–974. https://doi.org/10.1038/ni1488 PMID: 17581537

105. Malietzis G, Giacometti M, Kennedy RH, Athanasiou T, Aziz O, Jenkins JT. The emerging role of neutrophil to lymphocyte ratio in determining colorectal cancer treatment outcomes: a systematic review and meta-analysis. Ann Surg Oncol. 2014; 21(12):3938–3946. https://doi.org/10.1245/s10434-014-3815-2 PMID: 24866438

106. Walsh SR, Cook EJ, Goulder F, Justin TA, Keeling NJ. Neutrophil-lymphocyte ratio as a prognostic factor in colorectal cancer. J Surg Oncol. 2005; 91(3):181–184. https://doi.org/10.1002/jso.20329 PMID: 16118772

107. He JR, Shen GP, Ren ZF, Qin H, Cui C, Zhang Y, et al. Pretreatment levels of peripheral neutrophils and lymphocytes as independent prognostic factors in patients with nasopharyngeal carcinoma. Head Neck. 2012; 34(12):1769–76. https://doi.org/10.1002/hed.22008 PMID: 22318781

108. Krenn-Pilko S, Langsenlehner U, Thurner EM, Stojakovic T, Pichler M, Gerger A, et al. The elevated preoperative platelet-to-lymphocyte ratio predicts poor prognosis in breast cancer patients. Br J Cancer. 2014; 110(10):2524–2530. https://doi.org/10.1038/bjc.2014.163 PMID: 24675383

109. Pistelli M, Lisa MD, Ballatore Z, Caramanti M, Pagliacci A, Battelli N, et al. Pre-treatment neutrophil to lymphocyte ratio may be a useful tool in predicting survival in early triple negative breast cancer patients. BMC Cancer. 2015; 15:195. https://doi.org/10.1186/s12885-015-1204-2 PMID: 25884918

110. Halazun KJ, Hardy MA, Rana AA, Woodland DC, Luyten EJ, Mahadev S, et al. Negative impact of neutrophil-lymphocyte ratio on outcome after liver transplantation for hepatocellular carcinoma. Annals of Surgery. 2009; 250(1):141–151. https://doi.org/10.1097/SLA.0b013e3181a77e59 PMID: 19561458

111. Engblom C, Pfirschke C, Zilionis R, Martins JDS, Bos ASA, Courties G, et al. Osteoblasts remotely supply lung tumors with cancer-promoting SiglecFhigh neutrophils. Science. 2017; 358(6367): eaal5081. https://doi.org/10.1126/science.aal5081 PMID: 29191879

112. Bracarda S, Eggermont AM, Samuelsson J. Redefining the role of interferon in the treatment of malignant diseases. Eur J Cancer. 2010; 46(2):284–97. https://doi.org/10.1016/j.ejca.2009.10.013 PMID: 19906524

113. Chawla-Sarkar M, Lindner DJ, Liu YF, Williams BR, Sen GC, Silverman RH, et al. Apoptosis and interferons: role of interferon-stimulated genes as mediators of apoptosis. Apoptosis. 2003; 8(3):237–249. https://doi.org/10.1023/A:1023668705040 PMID: 12766484

114. Maeda S, Wada H, Naito Y, Nagano H, Simmons S, Kagawa Y, et al. Interferon-alpha acts on the S/G2/M phases to induce apoptosis in the G1 phase of an IFNAR2-expressing hepatocellular carcinoma cell line. J Biol Chem. 2014; 289(34):23786–95. https://doi.org/10.1074/jbc.M114.551879 PMID: 25012666

115. Rogge L, D'Ambrosio D, Biffi M, Penna G, Minetti LJ, Presky DH, et al. The role of Stat4 in species-specific regulation of Th cell development by type I IFNs. J Immunol. 1998; 161(12):6567–74. PMID: 9862683

116. Biron CA, Nguyen KB, Pien GC, Cousens LP, Salazar-Mather TP. Natural killer cells in antiviral defense: function and regulation by innate cytokines. Annu Rev Immunol. 1999; 17:189–220. https://doi.org/10.1146/annurev.immunol.17.1.189 PMID: 10358757

117. Salazar-Mather TP, Lewis CA, Biron CA. Type I interferons regulate inflammatory cell trafficking and macrophage inflammatory protein 1alpha delivery to the liver. J Clin Invest. 2002; 110(3):321–30. https://doi.org/10.1172/JCI15376 PMID: 12163451

118. Blanco P, Palucka AK, Gill M, Pascual V, Banchereau J. Induction of dendritic cell differentiation by IFN-alpha in systemic lupus erythematosus. Science. 2001; 294(5546):1540–1543. https://doi.org/10.1126/science.1064890 PMID: 11711679

119. Sistigu A, Yamazaki T, Vacchelli E, Chaba K, Enot DP, Adam J, et al. Cancer cell-autonomous contribution of type I interferon signaling to the efficacy of chemotherapy. Nat Med. 2014; 20(11):1301–1309. https://doi.org/10.1038/nm.3708 PMID: 25344738

120. Lim JY, Gerber SA, Murphy SP, Lord EM. Type I interferons induced by radiation therapy mediate recruitment and effector function of CD8(+) T cells. Cancer Immunol Immunother. 2014; 63(3):259–71. https://doi.org/10.1007/s00262-013-1506-7 PMID: 24357146

121. Oh SS, Moon C, Kim DH, Song H, Park S, Fu Y, et al. Adenovirally delivered IFN-β exerts antitumor effects through transient T-lymphocyte depletion and Ag-specific T-cell proliferation. Int J Mol Med. 2012; 29(6):1153–1157. https://doi.org/10.3892/ijmm.2012.936 PMID: 22426464

122. Huang H, Xiao T, Ji H, Liu XY. Interferon-*beta*-armed oncolytic adenovirus induces both apoptosis and necroptosis in cancer cells. Acta Biochim Biophys Sin(Shanghai). 2012; 44:737–745.

123. Park MY, Kim DR, Jung HW, Yoon HI, Lee JH, Lee CT. Genetic immunotherapy of lung cancer using conditionally replicating adenovirus and adenovirus-interferon-beta. Cancer Gene Ther. 2010; 17(5):356–64. https://doi.org/10.1038/cgt.2009.78 PMID: 19893592

124. Shih CS, Laurie N, Holzmacher J, Spence Y, Nathwani AC, Davidoff AM, et al. AAV-mediated local delivery of interferon-beta for the treatment of retinoblastoma in preclinical models. Neuromolecular Med. 2009; 11(1):43–52. https://doi.org/10.1007/s12017-009-8059-0 PMID: 19306089

125. Wakabayashi T, Natsume A, Hashizume Y, Fujii M, Mizuno M, Yoshida J. A phase I clinical trial of interferon-beta gene therapy for high-grade glioma: novel findings from gene expression profiling and autopsy. J Gene Med. 2008; 10(4):329–339. https://doi.org/10.1002/jgm.1160 PMID: 18220319

126. Kirkwood JM, Tarhini AA, Moschos SJ, Panelli MC. Adjuvant therapy with high-dose interferon alpha 2b in patients with high-risk stage IIB/III melanoma. Nat Clin Pract Oncol. 2008; 5(1):2–3. https://doi.org/10.1038/ncponc1004 PMID: 18030300

127. Amulic B, Cazalet C, Hayes GL, Metzler KD, Zychlinsky A. Neutrophil function: from mechanisms to disease. Annu Rev Immunol. 2012; 30:459–489. https://doi.org/10.1146/annurev-immunol-020711-074942 PMID: 22224774

128. Gabelloni ML, Trevani AS, Sabatte J, Geffner J. Mechanisms regulating neutrophil survival and cell death. Semin Immunopathol. 2013; 35(4):423–437. https://doi.org/10.1007/s00281-013-0364-x PMID: 23370701

129. Ibrahim SA, Kulshrestha A, Katara GK, Beaman KD. Delayed neutrophil apoptosis is regulated by cancer associated a2 isoform vacuolar ATPase. J Immunol. 2017; 198(1 Supplement):76.15.

130. Takeshima T, Pop LM, Laine A, Iyengar P, Hannan ESVR. Key role for neutrophils in radiation-induced antitumor immune responses: Potentiation with G-CSF. Proc Natl Acad Sci USA. 2016; 113(40):11300–11305. https://doi.org/10.1073/pnas.1613187113 PMID: 27651484

131. Grimes M, Hall B, Foltz L, Levy T, Rikova K, Gaiser J, et al. Integration of protein phosphorylation, acetylation, and methylation data sets to outline lung cancer signaling networks. Sci Signal. 2018; 11(531). https://doi.org/10.1126/scisignal.aaq1087 PMID: 29789295

132. Moroy G, Alix AJ, Sapi J, Hornebeck W, Bourguet E. Neutrophil elastase as a target in lung cancer. Anticancer Agents Med Chem. 2012; 12(6):565–79. https://doi.org/10.2174/187152012800617696 PMID: 22263788

133. Gong L, Cumpian AM, Caetano MS, Ochoa CE, la Garza MMD, Lapid DJ, et al. Promoting effect of neutrophils on lung tumorigenesis is mediated by CXCR2 and neutrophil elastase. Mol Cancer. 2013; 12(1):154. https://doi.org/10.1186/1476-4598-12-154 PMID: 24321240

134. Hattar K, Franz K, Ludwig M, Sibelius U, Wilhelm J, Lohmeyer J, et al. Interactions between neutrophils and non-small cell lung cancer cells: enhancement of tumor proliferation and inflammatory mediator synthesis. Cancer Immunol Immunother. 2014; 63(12):1297–306. https://doi.org/10.1007/s00262-014-1606-z PMID: 25186613

135. Aktas ON, Ozturk AB, Erman B, Erus S, Tanju S, Dilege S. Role of natural killer cells in lung cancer. J Cancer Res Clin Oncol. 2018; 144(6):997–1003. https://doi.org/10.1007/s00432-018-2635-3 PMID: 29616326

136. Revels SL, Lee JM. Anti-angiogenic therapy in nonsquamous non-small cell lung cancer (NSCLC) with tyrosine kinase inhibition (TKI) that targets the VEGF receptor (VEGFR): perspective on phase III clinical trials. J Thorac Dis. 2018; 10(2):617–620. https://doi.org/10.21037/jtd.2018.01.105 PMID: 29607123

137. Qu J, Zhang Y, Chen X, Yang H, Zhou C, Yang N. Newly developed anti-angiogenic therapy in non-small cell lung cancer. Oncotarget. 2017; 9(11):10147–10163. https://doi.org/10.18632/oncotarget.23755 PMID: 29515799

138. Stratigos M, Matikas A, Voutsina A, Mavroudis D, Georgoulias V. Targeting angiogenesis in small cell lung cancer. Transl Lung Cancer Res. 2016; 5(4):389–400. https://doi.org/10.21037/tlcr.2016.08.04 PMID: 27652203

139. Lee B, Konen J, Wilkinson S, Marcus AI, Jiang Y. Local alignment vectors reveal cancer cell-induced ECM fiber remodeling dynamics. Sci Rep. 2017; 7:39498. https://doi.org/10.1038/srep39498 PMID: 28045069

140. Siegelin MD, Borczuk AC. Epidermal growth factor receptor mutations in lung adenocarcinoma. Lab Invest. 2014; 94(2):129–137. https://doi.org/10.1038/labinvest.2013.147 PMID: 24378644

141. Liu X, Wang WP, Zhang C, Ma Z. Epidermal growth factor receptor (EGFR): A rising star in the era of precision medicine of lung cancer. Oncotarget. 2017; 8(30):50209–50220. https://doi.org/10.18632/oncotarget.16854 PMID: 28430586

142. Pyonteck SM, Akkari L, Schuhmacher AJ, Bowman RL, Sevenich L, Quail DF, et al. CSF-1R inhibition alters macrophage polarization and blocks glioma progression. Nat Med. 2013; 19(10):1264–72. https://doi.org/10.1038/nm.3337 PMID: 24056773

143. Houghton AM, Rzymkiewicz DM, Ji H, Gregory AD, Egea EE, Metz HE, et al. Neutrophil elastase-mediated degradation of IRS-1 accelerates lung tumor growth. Nat Med. 2010; 16(2):219–223. https://doi.org/10.1038/nm.2084 PMID: 20081861

144. Sangaletti S, Tripodo C, Vitali C, Portararo P, Guarnotta C, Casalini P, et al. Defective stromal remodeling and neutrophil extracellular traps in lymphoid tissues favor the transition from autoimmunity to lymphoma. Cancer Discov. 2014; 4(1):110–129. https://doi.org/10.1158/2159-8290.CD-13-0276 PMID: 24189145

145. Uribe-Querol E, Rosales C. Neutrophils in Cancer: Two Sides of the Same Coin. J Immunol Res. 2015; 2015::983698. https://doi.org/10.1155/2015/983698 PMID: 26819959

146. Arelaki S, Arampatzioglou A, Kambas K, Papagoras C, Miltiades P, Angelidou I, et al. Gradient Infiltration of Neutrophil Extracellular Traps in Colon Cancer and Evidence for Their Involvement in Tumour Growth. PLoS One. 2016; 11(5):e0154484. https://doi.org/10.1371/journal.pone.0154484 PMID: 27136460

147. Cools-Lartigue J, Spicer J, Najmeh S, Ferri L. Neutrophil extracellular traps in cancer progression. Cell Mol Life Sci. 2014; 71(21):4179–94. https://doi.org/10.1007/s00018-014-1683-3 PMID: 25070012

148. Demers M, Wagner DD. Neutrophil extracellular traps: A new link to cancer-associated thrombosis and potential implications for tumor progression. Oncoimmunology. 2013; 2(2):e22946. https://doi.org/10.4161/onci.22946 PMID: 23526174

149. Wculek SK, Malanchi I. Neutrophils support lung colonization of metastasis-initiating breast cancer cells. Nature. 2015; 528(7582):413–417. https://doi.org/10.1038/nature16140 PMID: 26649828

150. Tohme S, Yazdani HO, Al-Khafaji AB, Chidi AP, Loughran P, Mowen K, et al. Neutrophil Extracellular Traps Promote the Development and Progression of Liver Metastases after Surgical Stress. Cancer Res. 2016; 76(6):1367–1380. https://doi.org/10.1158/0008-5472.CAN-15-1591 PMID: 26759232

151. Kim Y, Stolarska M, Othmer HG. A hybrid model for tumor spheroid growth in vitro I: Theoretical development and early results. Math Models Methods in Appl Scis. 2007; 17:1773–1798. https://doi.org/10.1142/S0218202507002479

152. Kim Y, Stolarska M, Othmer HG. The role of the microenvironment in tumor growth and invasion. Prog Biophys Mol Biol. 2011; 106:353–379. https://doi.org/10.1016/j.pbiomolbio.2011.06.006 PMID: 21736894

153. Kim Y. Regulation of cell proliferation and migration in glioblastoma: New therapeutic approach. Frontiers in Molecular and Cellular Oncology. 2013; 3:53.

154. Kim Y, Roh S. A hybrid model for cell proliferation and migration in glioblastoma. Discrete and Continuous Dynamical Systems-B. 2013; 18(4):969–1015. https://doi.org/10.3934/dcdsb.2013.18.969

155. Kim Y, Othmer H. Hybrid models of cell and tissue dynamics in tumor growth. Math Bios Eng. 2015; 12(6):1141–1156. https://doi.org/10.3934/mbe.2015.12.1141

156. Kim Y, Powathil G, Kang H, Trucu D, Kim H, Lawler S, et al. Strategies of eradicating glioma cells: A multi-scale mathematical model with miR-451-AMPK-mTOR control. PLoS One. 2015; 10(1):e0114370. https://doi.org/10.1371/journal.pone.0114370 PMID: 25629604

157. Crestani B, Cornillet P, Dehoux M, Rolland C, Guenounou M, Aubier M. Alveolar type II epithelial cells produce interleukin-6 in vitro and in vivo. Regulation by alveolar macrophage secretory products. J Clin Invest. 1994; 94(2):731–40. https://doi.org/10.1172/JCI117392 PMID: 8040328

158. Yao X, Huang J, Zhong H, Shen N, Faggioni R, Fung M, et al. Targeting interleukin-6 in inflammatory autoimmune diseases and cancers. Pharmacol Ther. 2014; 141(2):125–39. https://doi.org/10.1016/j.pharmthera.2013.09.004 PMID: 24076269

159. Veldhoen M, Hocking RJ, Atkins CJ, Locksley RM, Stockinger B. TGF-β in the context of an inflammatory cytokine milieu supports de novo differentiation of IL-17-producing T cells. Immunity. 2006; 24(2):179–189. https://doi.org/10.1016/j.immuni.2006.01.001 PMID: 16473830

160. Korn T, Bettelli E, Gao W, Awasthi A, Jäger A, Strom TB, et al. IL-21 initiates an alternative pathway to induce proinflammatory T_H17 cells. Nature. 2007; 448(7152):484–487. https://doi.org/10.1038/nature05970 PMID: 17581588

161. Piccard H, Muschel RJ, Opdenakker G. On the dual roles and polarized phenotypes of neutrophils in tumor development and progression. Crit Rev Oncol Hematol. 2012; 82(3):296–309. https://doi.org/10.1016/j.critrevonc.2011.06.004 PMID: 21798756

162. Ardi VC, Kupriyanova TA, Deryugina EI, Quigley JP. Human neutrophils uniquely release TIMP-free MMP-9 to provide a potent catalytic stimulator of angiogenesis. Proc Natl Acad Sci USA. 2007; 104(51):20262–20267. https://doi.org/10.1073/pnas.0706438104 PMID: 18077379

163. Coussens LM, Tinkle CL, Hanahan D, Werb Z. MMP-9 supplied by bone marrow-derived cells contributes to skin carcinogenesis. Cell. 2000; 103(3):481–90. https://doi.org/10.1016/S0092-8674(00)00139-2 PMID: 11081634

164. Acuff HB, Carter KJ, Fingleton B, Gorden DL, Matrisian LM. Matrix metalloproteinase-9 from bone marrow-derived cells contributes to survival but not growth of tumor cells in the lung microenvironment. Cancer Res. 2006; 66(1):259–66. https://doi.org/10.1158/0008-5472.CAN-05-2502 PMID: 16397239

165. Masson V, d l Ballina LR, Munaut C, Wielockx B, Jost M, Maillard C, et al. Contribution of host MMP-2 and MMP-9 to promote tumor vascularization and invasion of malignant keratinocytes. FASEB J. 2005; 19(2):234–6. https://doi.org/10.1096/fj.04-2140fje PMID: 15550552

166. Welch DR, Schissel DJ, Howrey RP, Aeed PA. Tumor-elicited polymorphonuclear cells, in contrast to normal circulating polymorphonuclear cells, stimulate invasive and metastatic potentials of rat mammary adenocarcinoma cells. Proc Natl Acad Sci U S A. 1989; 86(15):5859–63. https://doi.org/10.1073/pnas.86.15.5859 PMID: 2762301

167. Romani L, Mencacci A, Cenci E, Spaccapelo R, Sero GD, Nicoletti I, et al. Neutrophil production of IL-12 and IL-10 in candidiasis and efficacy of IL-12 therapy in neutropenic mice. J Immunol. 1997; 158(11):5349–56. PMID: 9164955

168. Curiel TJ. Tregs and rethinking cancer immunotherapy. J Clin Invest. 2007; 117(5):1167–117. https://doi.org/10.1172/JCI31202 PMID: 17476346

169. Bach JF. Regulatory T cells under scrutiny. Nat Rev Immunol. 2003; 3:189–198. https://doi.org/10.1038/nri1026 PMID: 12658267

170. Shevach EM. CD4+ CD25+ suppressor T cells: more questions than answers. Nat Rev Immunol. 2002; 2:389–400. https://doi.org/10.1038/nri821 PMID: 12093005

171. Levings MK, Sangregorio R, Roncarolo MG. Human CD25(+)CD4(+) T regulatory cells suppress naive and memory T cell proliferation and can be expanded in vitro without loss of function. J Exp Med. 2001; 193(11):1295–302. https://doi.org/10.1084/jem.193.11.1295 PMID: 11390436

172. Wang RF. Immune suppression by tumor-specific CD4+ regulatory T-cells in cancer. Semin Cancer Biol. 2006; 16(1):73–9. https://doi.org/10.1016/j.semcancer.2005.07.009 PMID: 16140545

173. Wang RF, Peng G, Wang HY. Regulatory T cells and Toll-like receptors in tumor immunity. Semin Immunol. 2006; 18(2):136–42. https://doi.org/10.1016/j.smim.2006.01.008 PMID: 16469504

174. Chen ML, Pittet MJ, Gorelik L, Flavell RA, Weissleder R, von Boehmer H, et al. Regulatory T cells suppress tumor-specific CD8 T cell cytotoxicity through TGF-beta signals in vivo. Proc Natl Acad Sci USA. 2005; 102:419–424. https://doi.org/10.1073/pnas.0408197102 PMID: 15623559

175. Fu S, Zhang N, Yopp AC, Chen D, Mao M, Chen D, et al. TGF-beta induces Foxp3 + T-regulatory cells from CD4 + CD25 - precursors. Am J Transplant. 2004; 4(10):1614–27. https://doi.org/10.1111/j.1600-6143.2004.00566.x PMID: 15367216

176. Ni XY, Sui HX, Liu Y, Ke SZ, Wang YN, Gao FG. TGF-beta of lung cancer microenvironment upregulates B7H1 and GITRL expression in dendritic cells and is associated with regulatory T cell generation. Oncol Rep. 2012; 28(2):615–21. https://doi.org/10.3892/or.2012.1822 PMID: 22614805

177. Kinoshita T, Ishii G, Hiraoka N, Hirayama S, Yamauchi C, Aokage K, et al. Forkhead box P3 regulatory T cells coexisting with cancer associated fibroblasts are correlated with a poor outcome in lung adenocarcinoma. Cancer Sci. 2013; 104(4):409–15. https://doi.org/10.1111/cas.12099 PMID: 23305175

178. Tao L, Huang G, Song H, Chen Y, Chen L. Cancer associated fibroblasts: An essential role in the tumor microenvironment. Oncol Lett. 2017; 14(3):2611–2620. https://doi.org/10.3892/ol.2017.6497 PMID: 28927027

179. Choe C, Shin YS, Kim C, Choi SJ, Lee J, Kim SY, et al. Crosstalk with cancer-associated fibroblasts induces resistance of non-small cell lung cancer cells to epidermal growth factor receptor tyrosine kinase inhibition. Onco Targets Ther. 2015; 8:3665–3678. https://doi.org/10.2147/OTT.S89659 PMID: 26676152

180. Wang Z, Lin S, Li JJ, Xu Z, Yao H, Zhu X, et al. MYC protein inhibits transcription of the microRNA cluster MC-let-7a-1—let-7d via noncanonical e-box. Journal of Biological Chemistry. 2011; 286(46):39703–39714. https://doi.org/10.1074/jbc.M111.293126 PMID: 21903590

181. Takamizawa J, Konishi H, Yanagisawa K, Tomida S, Osada H, Endoh H, et al. Reduced expression of the let-7 microRNAs in human lung cancers in association with shortened postoperative survival. Cancer Research. 2004; 64(11):3753. https://doi.org/10.1158/0008-5472.CAN-04-0637 PMID: 15172979

182. Johnson SM, Grosshans H, Shingara J, Byrom M, Jarvis R, Cheng A, et al. RAS is regulated by the let-7 microRNA family. Cell. 2005; 120(5):635–647. https://doi.org/10.1016/j.cell.2005.01.014 PMID: 15766527

183. Mitselou A, Batistatou A, Nakanishi Y, Hirohashi S, Vougiouklakis T, Charalabopoulos K. Comparison of the dysadherin and E-cadherin expression in primary lung cancer and metastatic sites. Histology and Histopathology. 2010; 25(10):1257–1267. https://doi.org/10.14670/HH-25.1257 PMID: 20712010

184. Roberts P, Der C. Targeting the Raf-MEK-ERK mitogen-activated protein kinase cascade for the treatment of cancer. Oncogene. 2007; 26(22):3291–3310. https://doi.org/10.1038/sj.onc.1210422 PMID: 17496923

185. Zhao C, Du G, Skowronek K, Frohman MA, Bar-Sagi D. Phospholipase D2-generated phosphatidic acid couples EGFR stimulation to Ras activation by Sos. Nature Cell Biology. 2007; 9(6):707–712. https://doi.org/10.1038/ncb1594

186. Brown KS, Hill CC, Calero GA, Myers CR, Lee KH, Sethna JP, et al. The statistical mechanics of complex signaling networks: nerve growth factor signaling. Physical Biology. 2004; 1:184. https://doi.org/10.1088/1478-3967/1/3/006 PMID: 16204838

187. Huang S, Ren X, Wang L, Zhang L, Wu X. Lung-cancer chemoprevention by induction of synthetic lethality in mutant KRAS premalignant cells in vitro and in vivo. Cancer Prevention Research. 2011; 4(5):666. https://doi.org/10.1158/1940-6207.CAPR-10-0235 PMID: 21543344

188. Bettelli E, Carrier Y, Gao W, Korn T, Strom TB, Oukka M, et al. Reciprocal developmental pathways for the generation of pathogenic effector T_H17 and regulatory T cells. Nature. 2006; 441(7090):235–238. https://doi.org/10.1038/nature04753 PMID: 16648838

189. Abulaiti A, Shintani Y, Funaki S, Nakagiri T, Inoue M, Sawabata N, et al. Interaction between non-small-cell lung cancer cells and fibroblasts via enhancement of TGF-beta signaling by IL-6. Lung Cancer. 2013; 82(2):204–13. https://doi.org/10.1016/j.lungcan.2013.08.008 PMID: 24011634

190. Tirino V, Camerlingo R, Bifulco K, Irollo E, Montella R, Paino F, et al. TGF-β1 exposure induces epithelial to mesenchymal transition both in CSCs and non-CSCs of the A549 cell line, leading to an increase of migration ability in the CD133+ A549 cell fraction. Cell Death Dis. 2013; 4:e620. https://doi.org/10.1038/cddis.2013.144 PMID: 23640462

191. Borregaard N. Neutrophils, from marrow to microbes. Immunity. 2010; 33:657–70. https://doi.org/10.1016/j.immuni.2010.11.011 PMID: 21094463